INVESTIGATION OF DEFORMATION AND SHAPE MEMORY CHARACTERISTICS OF THERMOPLASTIC POLYMERS

A THESIS SUBMITTED TO
THE GRADUATE SCHOOL OF NATURAL AND APPLIED SCIENCES
OF
MIDDLE EAST TECHNICAL UNIVERSITY

BY

CİHAN YİĞİTBAŞI

IN PARTIAL FULFILLMENT OF THE REQUIREMENTS
FOR
THE DEGREE OF MASTER OF SCIENCE
IN
MECHANICAL ENGINEERING

JUNE 2018

Approval of the thesis:

INVESTIGATION OF DEFORMATION AND SHAPE MEMORY CHARACTERISTICS OF THERMOPLASTIC POLYMERS

submitted by **CİHAN YİĞİTBAŞI** in partial fulfillment of the requirements for the degree of **Master of Science in Mechanical Engineering Department, Middle East Technical University** by,

Prof. Dr. Halil Kalıpçılar _____
Dean, Graduate School of **Natural and Applied Sciences**

Prof. Dr. M.A.Sahir Arıkan _____
Head of Department, **Mechanical Engineering**

Assist. Prof. Dr. Hüsnü Dal _____
Supervisor, **Mechanical Engineering Department, METU**

Examining Committee Members:

Prof. Dr. Serkan Dağ
Mechanical Engineering Department, METU _____

Assist. Prof. Dr. Hüsnü Dal
Mechanical Engineering Department, METU _____

Assoc. Prof. Dr. Ercan Gürses
Aerospace Engineering Department, METU _____

Assoc. Prof. Dr. Murat Demiral
Mechanical Engineering Department, UTAA _____

Assist. Prof. Dr. Sezer Özerinç
Mechancal Engineering Department, METU _____

Date: **21.06.2018**

I hereby declare that all information in this document has been obtained and presented in accordance with academic rules and ethical conduct. I also declare that, as required by these rules and conduct, I have fully cited and referenced all material and results that are not original to this work.

Name, Last Name: CİHAN YİĞİTBAŞI

Signature :

ABSTRACT

INVESTIGATION OF DEFORMATION AND SHAPE MEMORY CHARACTERISTICS OF THERMOPLASTIC POLYMERS

YİĞİTBAŞI, Cihan
M.S., Department of Mechanical Engineering
Supervisor : Assist. Prof. Dr. Hüsnü Dal

JUNE 2018, 62 pages

Algorithmic implementation of constitutive models for shape memory polymers into commercial software packages through user material interfaces is the subject of this thesis. The effect of temperature change on the behaviors of these materials has been examined. The formulation of the generated material model has been constructed in the logarithmic strain space. Material model structure consists of three main steps. (i) In the geometric pre-processing step, using current and plastic metric, total and plastic logarithmic strain measures were defined, respectively. (ii) In the material model step, constitutive equations for (an)isotropic elasto viscoplasticity in the logarithmic strain space were identified in a structure analogous to geometrically linear theory. (iii) In geometric post-processor step, the objects obtained in logarithmic strain space were mapped back to their nominal, Eulerian or Lagrangian counterparts. After these three main stages, the 8-chain model with the double kink theory was used to define the flow rule for plastic strain in logarithmic strain space. All the material information that was theoretically defined was written as a FORTRAN code. A new term has been added to the tangent moduli calculations in order to run this code in ABAQUS. The obtained material model was verified by comparing with the test data in the literature. Finally, the shape memory effect of thermoplastic materials on a tube geometry is investigated in ABAQUS. The results suggest significant shape memory effect for plexiglass.

Keywords: thermoplastic polymers, shape memory characteristics, finite element model, user material routine, finite thermoviscoplasticity, logarithmic strain

ÖZ

TERMOPLASTİK POLİMERLERİN DEFORMASYON VE ŞEKİL HAFIZA ÖZELLİKLERİNİN İNCELENMESİ

YİĞİTBAŞI, Cihan
Yüksek Lisans, Makina Mühendisliği Bölümü
Tez Yöneticisi : Dr. Öğr. Üyesi Hüsnü Dal

Haziran 2018 , 62 sayfa

Ticari yazılımların kullanıcı malzeme arayüzleri kullanılarak şekil hafızalı polimerlerin algoritmik yaklaşımlarla temel özelliklerinin bu yazılımlara aktarılması bu tezin konusudur. Bu malzemelerin davranışlarında sıcaklık değişiminin etkisi incelenmiştir. Ortaya konulan malzeme modelinin formülasyonu, logaritmik gerinim uzayında oluşturulmuştur. Malzeme model yapısı üç ana adımdan oluşmaktadır. (i) Geometrik ön işleme aşamasında, mevcut ve plastik metrik kullanılarak, sırasıyla toplam ve plastik logaritmik gerilme ölçüleri tanımlanmıştır. (ii) Malzeme modeli aşamasında, (an)izotrop elasto viskoplastisite için geometrik olarak doğrusal teoriye benzer bir yapıda malzeme modeli denklemleri logaritmik gerinim uzayında tanımlanmıştır. (iii) Geometrik son işlemci aşamasında, logaritmik gerinim uzayında elde edilen nesneler nominal, Eulerian ve Lagrangian karşılıklarına haritalanmıştır. Bu üç ana aşamadan sonra, 8-chain model double kink teori ile kullanılarak logaritmik gerinim uzayındaki plastik gerinim akış kuralı tanımlanmıştır. Teorik olarak tanımlanan tüm bu malzeme bilgileri FORTRAN kodu olarak yazılmıştır. Yazılan bu kodu ABAQUS'te çalıştırabilmek için tanjant modül hesaplamalarında yeni bir terim eklenmiştir. Elde edilen malzeme modeli literatürdeki test datalarıyla karşılaştırma yapılarak doğrulanmıştır. Son olarak, bir tüp geometrisi üzerinde termoplastik malzemelerin şekil hafıza etkisi ABAQUS'te incelenmiştir. Sonuçlar pleksiglas için önemli şekil hafıza etkisi belirtir.

Anahtar Kelimeler: termoplastik polimerler, şekil hafıza özellikleri, sonlu eleman modeli, kullanıcı malzeme rutini, sonlu termoviskoplastisite, logaritmik gerinim

To my love Selen

ACKNOWLEDGMENTS

I would like to express my gratitude to my supervisor Assist. Prof. Dr. Hüsnü Dal for his worthwhile guidance, precious advices and encouragements through my study. Without his valuable support it would be very hard for me to study with full motivation and willingness.

I would like to thank my mother, father and brothers who have always supported me in all my life.

More than all, I would like to express my very special thanks to my love Selen Temel Yiğitbaşı for her endless support, encouragement, patience and love.

TABLE OF CONTENTS

LIST OF TABLES

TABLES

LIST OF FIGURES

FIGURES

LIST OF ABBREVIATIONS

UMAT	User Defined Material Routine
SMPs	Shape Memory Polymers
T_g	Glass Transition Temperature
CDI	Clausius-Duhem Inequality
CPI	Clausius-Planck Inequality
FI	Fourier Inequality
PMMA	Poly Methyl Methacrylate

CHAPTER 1

MOTIVATION AND OVERVIEW

This chapter provides an overview of shape memory polymers (SMPs). In the first section, general information about SMPs will be given. History of SMPs and application regions are also mentioned in this section. The second section is devoted to the aim of the thesis. In the third and fourth sections, literature review and structure of the work will be explained, respectively.

1.1 Shape Memory Polymers

1.1.1 Introduction

SMP is called as a smart material. Temporary shape of this material is given upon deformation and material returns back to its original shape by external stimulus such as heat, electricity and magnetism. Temperature change is one of the most widely used external stimulus for SMPs which store shapes and retrieves its former shape changing temperature.

Dual shape property of SMPs has increased its popularity in the recent times. Other features of SMPs, which are listed below, also led research groups to focus on this area. They are

- response to external stimuli
- simpler design than conventional ones
- more compact
- more efficient

- recover large deformation
- low fabrication cost
- adjustable recovery temperature
- low weight
- potential biocompatibility
- biodegradability
- excellent manufacturability

Liu et al. [41] classified the shape memory materials according to their shape fixing and recovery capability as seen in Figure 1.1. The diagram was plotted as strain versus temperature change. Detailed information about shape fixing and shape recovery will be given in Section 1.3. In Figure 1.1(a), ideal shape memory material can be seen. The recovery of material occurs at constant temperature value. In Figure 1.1(b), the material has an perfect shape fixing and recovery, however, there is a sharp change between fixing and recovery step. In Figure 1.1(c), the material has great shape recovery with insufficient shape fixing. In Figure 1.1(d), the material has perfect shape fixing with lack of shape recovery. Moreover, there is another shape memory material as both insufficient shape fixing and recovery that is not included in the figure.

1.1.2 History of Shape Memory Polymers

In 1941, a patent issued by L. B. Vernon mentions the term *"elastic memory"* [1]. According to this patent, a dental material consist of methacrylic acid ester resin has an *"elastic memory"*. When heated, this material returns to its original state. This is the first time recognition of shape memory effect.
Until the 1960s, the significance of shape memory polymers was not noticed. The well-known heat shrinkage tubing emerged in these years [2].
The first shape memory polymer, polynorbornene-based polymer, was used in 1984 by CDF Chimie, a French company [3]. In the same year, it was used as a commercial product by the Japanese Nippon Zeon company under the name of Narsonex [4]. The glass transition temperature T_g of this polymer is between 35 °C and 40 °C and the application area is limited due to processibility.

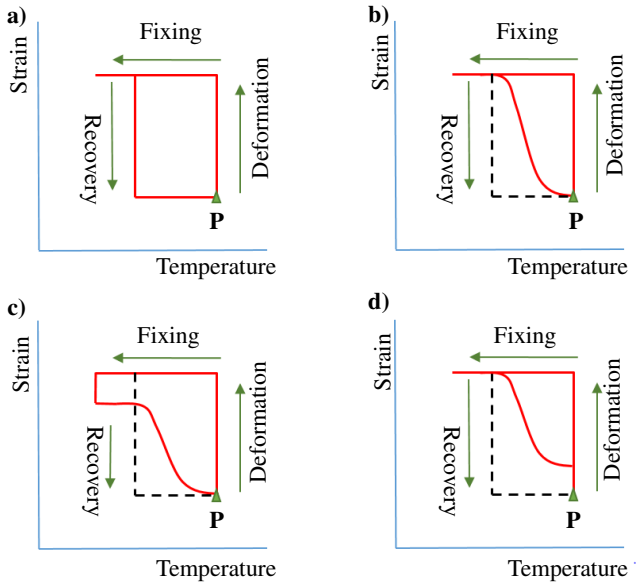

Figure 1.1: Type of shape memory polymers from their shape fixing and recovery capabilities. Starting point of the cycle is point **P** [32]. a) Shape memory polymer in ideal type. b) Perfect shape fixing and recovery type shape memory polymers. c) Great shape recovery and insufficient shape fixing type shape memory polymers. d) Perfect shape fixing and insufficient shape recovery type shape memory polymers.

The second commercial shape memory polymer Kurare TP-301 was developed by Japanese The Kurare Corporation. This poly (trans-isoprene) based polymer has a melting temperature of 67 °C degrees and a T_g of -68 °C. This polymer also has limited processability such as polynorbornene [5].

The third commercial a poly (styrene-butadiene) based shape memory polymer, Asmer, was put on the market by the Japanese Asahi Company. It has an range of 60 °C to 90 °C T_g value [5].

By the end of 1980s, segmented polyurethane shape memory polymer was developed by Mitsubishi Heavy Industry [6].

In the 1990s, the development and use of polyurethane became widespread. Under favour of the properties, such as varying T_g values and controlling the structure have led to an increase in the potential application areas of polyurethane and increase the importance of polyurethane in the industry. In addition, polyurethane is thermoplastic polymer, which shows good processability.

1.1.3 Application Regions of SMP

Shape memory polymers have recently exposed to considerable attention from designers. The reason for this interest is that mechanical features of these materials change by external stimulus. This stiation has greatly increased the use of shape memory polymers. In this section, we will give a few examples of usage areas of SMPs.

1.1.3.1 Clothing Materials

The properties of water vapor permeability vary according to the properties of polymeric materials used in clothing. For instance, as the temperature increases, the permeability of the raincoats increases and this ensures a comfortable use. Such polymers are used in items such as raincoat, inner soles and boot covering.

1.1.3.2 Medical Devices

SMPs are widely used in medical applications such as removal of blood clots. First, laser-activated device is used to enter the vessel where the clot placed. With the aid of the laser, material changes to its original shape like spring. Then, the clot is extracted from the vessel [7].
Biodegradable SMPs are used for stitching a wound. After the stitching operation, the suture returns to its original state with the body temperature and the stitches become firm [7]. Since the biodegradable feature of the suture emerged after a certain period of time, there is no need for an operation to take the suture.
SMP stents are also used to prevent vascular occlusions. These stents are placed where the occlusion is occur, and as the temperature increases, the stent returns to its original shape. Thus, extension of vessel supplies easy blood flow.

1.1.3.3 Structures

The properties of SMPs such as low mass, low volume, low cost, depoyable structures for space and commercial applications have been confirmed [8]. For instance, the damping property of the material can be determined by controlling the temperature of the SMP in the fiber reinforcement composite. This can reduce the noise produced on defense system platforms. Second example is an inflatable truss frame in space applications, which gives better results than current state-of-the-art truss frame [9].

1.2 Aim of the Thesis

The application areas of shape memory polymers are increasing day by day. The eligible features of these materials cause this increase. The industry has not been insensitive to this development. However, the material library of the existing finite element programs is not sufficient for modeling these smart materials. For this reason, it became apparent that these smart materials had to be added to the commercial finite element model programs. This thesis is devoted to create constitutive model to investigate deformation and shape memory characteristics of thermoplastic polymer, poly (methyl methacrylate) (PMMA) which is also glassy polymer, and transfer this model to commercial finite element model program ABAQUS. Temperature change effect in the material model will be examined.

1.3 Literature Review

Shape memory polymers have an important position in the research world due to their superior properties comparing other materials and to be an smart material. In the literature, there may be many articles about the behavior of these materials and how these behaviours change thanks to external stimulus. A few of these articles which also include implementation of the constitutive models in a finite element setup will be provided in this section.

A three dimensional finite strain phenomenological model for thermo responsive shape memory polymers was proposed from Boatti et al. [32]. In this article, ther-

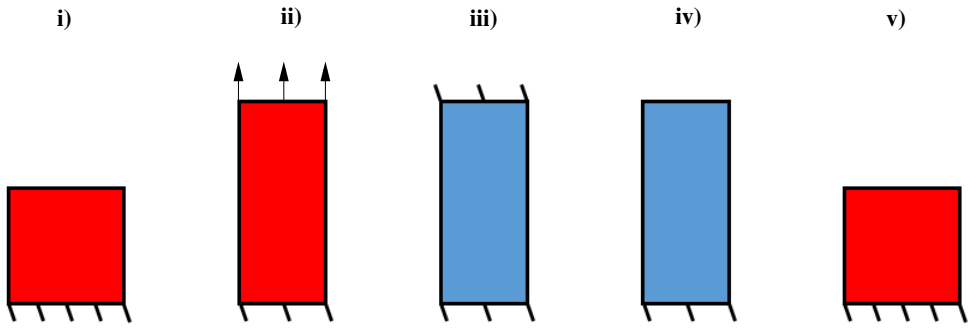

Figure 1.2: High temperature shape fixing and shape recovery. i) Material in high temperature. ii) Deformed material at high temperature. iii) Cooling the material while constraining. iv) Unloading of material. v) Heating for shape recovery.

modynamically consistent, three dimensional formulated constitutive model valid in large deformations was created. The material model was implemented into the ABAQUS using user material routine (UMAT). In order to validate the material model, the test anaylsis were done. For these test analysis, the shape memory cycle which consists of two steps such as shape fixing and shape recovery was applied. According to Lendlein et al. [35] there are two ways to get shape fixing. One of them is high temperature shape fixing seen in Figure 1.2 and other is low temperature shape fixing seen in Figure 1.3. Shape fixing in high temperature condition, firstly the material is deformed at higher temperatures than the transition temperature. After that, the part is cooled while constraining. Finally, the part is unloaded. On the other hand, shape fixing in low temperature condition, the material is deformed at less than transition temperature and unloaded. After both shape fixing operations, material is heated in order to obtain original shape. Comparing the shape fixing alternatives for huge parts, low temperature shape fixing has an advantage because there is no extra heating step required. The results, obtained for these two shape memory cycle, were compared with the test data from the literature [33] and [34].

Baghani et al. [36] described an another three dimensional large strain macromechanical model which uses the logarithmic (or Hencky) strain. They took the advantage of the decomposition of logarithmic strain tensor as rubbery and glassy parts and multiplicative decomposition of the deformation gradient in their constitutive model. Validation of the constitutive model was verified by the uniaxial test data taken from literature. They also checked the difference of large and small strain theory by the

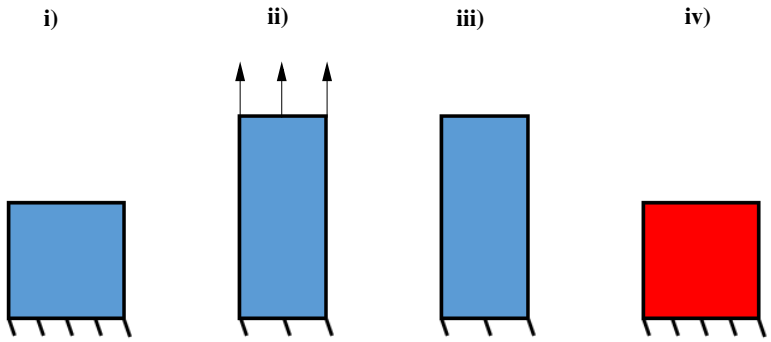

Figure 1.3: Low temperature shape fixing and shape recovery. i) Material in low temperature. ii) Deformed material at low temperature. iii) Unloading of material. iv) Heating for shape recovery.

help of simple shear analysis. All the analysis were done in ABAQUS with the UMAT interface. The main purpose of the Baghani et al. [36] was to develope a Hencky based finite deformation model which considers large deformation effect.

Qi et al. [37] proposed phase transition based three dimensional constitutive model to identify finite deformation thermo-mechanical behaviours of amorphous shape memory polymers. By doing experiments, they wanted to understand the material characteristics of shape memory polymers. The created material model was compared with the results of thermo-mechanical experiments. For this comparison, the material model was implemented in UMAT in the finite element program ABAQUS. The tests were done for different temperatures with different strain rates. Proposed material model showed good similarity with test results. Free recovery and constraint recovery cases of material model were also compared, however, experimental data had an good match with only free recovery data.

Srivastava et al. [38] developed a thermo-mechanically coupled large deformation constitutive theory by using the classical Kröner Lee multiplicative decomposition of the deformation gradient. They made an large strain compression experiments with varying temperature and strain rates in order to calibrate the material parameters. Obtained material model was implemented into ABAQUS via UMAT interface. The model was validated with comparing the changing temperature and strain rate experimental data. Lastly, they implemented the material model in ABAQUS to simulate behaviour of shape memory polymer stent.

Diani et al. [39] described a material model to show shape recovery characteristics of

amorphous polymers which depends on the material viscoelasticity and its time temperature dependence. They have used Maxwell model with Williams-Landel-Ferry (WLF) equation. This model and equation are available in ABAQUS. For this reason, specified parameters directly implemented into ABAQUS. Instead of uniaxial tension or compression test, shape recovery model was validated with torsion test which has an non-homogenous strain and stresses. In addition, time and temperature dependence of shape recovery was shown by torsion analysis of a bar in ABAQUS.
Reese et al. [40] formulated thermomechanical modelling of shape memory polymers in macromechanical and micromechanical format in order to get connection between microstructure of rubberlike materials and the theoretical model. There was no result comparison with test data because, the main aim was development of material model. Obtained constitutive model was implemented into finite element software "FEAP" which was developed at the University of California at Berkeley. Finally, thermo-mechanical response of shape memory stent was investigated in this article.

1.4 Structure of the Work

Chapter 2 deals with fundamentals of continuum mechanics. Basic geometic mappings at finite strains and balance laws are briefly discussed. Local and conductive parts of dissipation are defined. Chapter 3 includes the kinematical approaches to the modeling of large viscoplastic deformation behaviour of glassy polymers. Kröner-Lee decomposition of the deformation gradient was used. Departing from the modular kinematic formulation in the logarithmic strain space which was proposed from Miehe et al. [14], the definitions for the modeling of glassy polymers have been done. Chapter 4 represents the thermoviscoplastic constitutive model characteristics of glassy polymers. Viscoplastic flow rule, stress, tangent moduli and thermal softening mechanisms of material model have been defined here. Chapter 5 is devoted the algorithmic implementation of the model. Update of internal variables and tangent moduli were identified. All the steps for the algorithmic setting were summarized in this chapter. Chapter 6 is concerned with the comparison of experimental results and analysis results to show validation of the material model. Moreover, modeling capability of written constitutive model was shown with numerical examples in detail.

CHAPTER 2

INTRODUCTION TO CONTINUUM MECHANICS

Basic equations of continuum mechanics are mentioned in this chapter. In addition, the key ingredients of thermodynamics which describe the thermomechanics of an inelastic solid are also considered. All the notions shown here are well qualified in literature. For more detailed information, please refer to references [10], [11], [12].

2.1 Fundamental Geometric Mappings

Let us consider a body, $\mathcal{B}$ at a reference time $t = t_0$ and points in that body are called as material points which are expressed as $\boldsymbol{X} \in \mathbb{R}^3$ Likewise, $\mathcal{S}_t$ is the region of space occupied by the body $\mathcal{B}$ at time t and points in that body is named as spatial points which are expressed as $\boldsymbol{x} \in \mathbb{R}^3$. The motion of the body $\mathcal{B}$ is a smooth function $\boldsymbol{\varphi}$ that assigns to each material point $\boldsymbol{X}$ and time t a point. Then, the function

$$\boldsymbol{\varphi}(\boldsymbol{X}, t) = \begin{cases} \mathcal{B} \ \rightarrow \ \mathcal{S}_t \\ \boldsymbol{X} \ \rightarrow \ \boldsymbol{x} = \boldsymbol{\varphi}(\boldsymbol{X}, t) \end{cases} \tag{2.1}$$

is stated as the deformation map, see Figure 2.1. The deformation gradient

$$\boldsymbol{F} = \frac{\partial \boldsymbol{\varphi}(\boldsymbol{X}, t)}{\partial \boldsymbol{X}} = \frac{\partial \boldsymbol{x}}{\partial \boldsymbol{X}} \tag{2.2}$$

linearly maps the line element $d\boldsymbol{X}$ onto its spatial counterpart $d\boldsymbol{x}$.

The cofactor $\mathrm{cof}[\boldsymbol{F}] = \det \boldsymbol{F}\boldsymbol{F}^{-T}$ of the deformation gradient $\boldsymbol{F}$ maps area vectors $d\boldsymbol{A}$ of material surfaces onto area vectors $d\boldsymbol{a}$ of the associated deformed spatial surfaces.

The Jacobian $J = \det \boldsymbol{F}$ maps the material volume dV onto spatial volume dv. The motion of a body is unique and uniquely invertible. This is guaranteed if the Jacobian

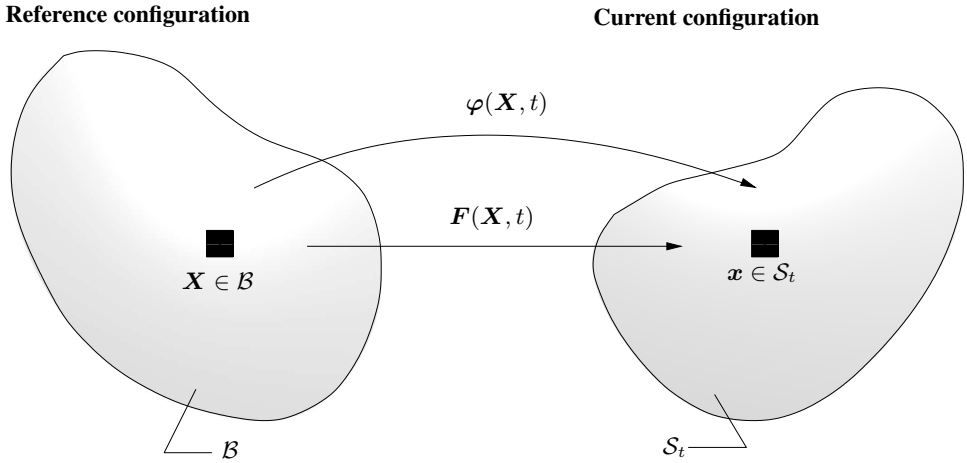

Figure 2.1: Material and spatial manifolds of a continuous body

is nonzero. The Jacobian is also always positive, which suggests that map is real. Lagrangian and Eulerian metrics are defined to measure objects in reference and spatial configurations

$$\boldsymbol{G} : T_X\mathcal{B} \rightarrow T_X^*\mathcal{B} \qquad \text{and} \qquad \boldsymbol{g} : T_x\mathcal{S} \rightarrow T_x^*\mathcal{S}, \tag{2.3}$$

respectively. Pull-back of the current metric $\boldsymbol{g}$ into the reference configuration gives the right Cauchy-Green deformation tensor as

$$\boldsymbol{C} = \boldsymbol{F}^T\boldsymbol{g}\boldsymbol{F} \tag{2.4}$$

The left Cauchy-Green deformation tensor is the inverse of reference metric in Eulerian configuration

$$\boldsymbol{b} = \boldsymbol{c}^{-1} = \boldsymbol{F}\boldsymbol{G}^{-1}\boldsymbol{F}^T. \tag{2.5}$$

The Lagrangian metric $\boldsymbol{G}$ and the Eulerian counterpart $\boldsymbol{g}$ are considered to be mappings between tangential and cotangential spaces. The geometric mappings between the tangential and cotangential spaces of the Lagrangian and Eulerian configurations are shown in the Figure 2.2 .

2.2 Balance Laws

The study of fundamental laws of physics as applied to mechanical systems is the topic of this section. The laws or principles of physics will be studied here in briefly.

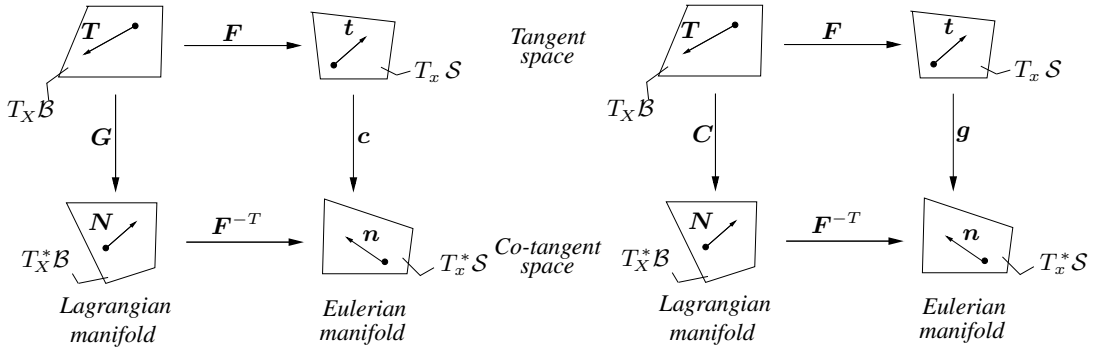

Figure 2.2: Geometric mappings between tangent and cotangent spaces of the Lagrangian and Eulerian configurations

All calculations are done for a unit volume of current configuration, that detailed information can be found in the book [12].

2.2.1 Conservation of Mass

The total mass in a closed system is always fixed and does not alter in any motion. Therefore;

$$\boxed{m = \int_{\mathcal{S}_t} \rho dv = \int_{\mathcal{B}} \rho_0 dV = constant \quad \Rightarrow \quad \frac{dm}{dt} = 0} \tag{2.6}$$

The continuity equation which shows local conservation of mass at any point in a continuous medium is expressed as

$$\boxed{\frac{d\rho}{dt} + \rho \operatorname{div} \boldsymbol{v} = 0}, \tag{2.7}$$

where ρ, ρ_0 and $\boldsymbol{v}$ are the current density, reference density and the spatial velocity, respectively.

2.2.2 Conservation of Momentum

The temporal change in the body's momentum is equal to the sum of the forces acting on the body in the immediate vicinity and from the distance. Thus, conservation of momentum is given as

$$\boxed{\frac{d}{dt}\int_{\mathcal{S}_t} \rho \boldsymbol{v} dv = \int_{\mathcal{S}_t} \rho \boldsymbol{b} dv + \int_{\mathcal{S}_t} \boldsymbol{t} dA}. \tag{2.8}$$

The Cauchy's theorem states that

$$\boxed{\boldsymbol{t} = \boldsymbol{\sigma}\boldsymbol{n}}, \tag{2.9}$$

where $\boldsymbol{b}$ is the body forces per unit deformed volume, $\boldsymbol{t}$ is the surface traction per unit deformed area and $\boldsymbol{\sigma}$ is the Cauchy stress tensor. Combining equations (2.7) and (2.8), the local form of the momentum balance expression is obtained

$$\boxed{\rho\dot{\boldsymbol{v}} = \operatorname{div}\boldsymbol{\sigma} + \rho\boldsymbol{b}}. \tag{2.10}$$

2.2.3 Conservation of Moment of Momentum

The conservation of angular momentum states that the net moment acting on the body is balanced by the temporal changes in the angular momentum. Local form of balance of angular momentum demands that the Cauchy stress is symmetric

$$\boxed{\boldsymbol{\sigma} = \boldsymbol{\sigma}^T}. \tag{2.11}$$

As a result, the local form of balance of angular momentum demands

$$\boxed{\boldsymbol{\tau} = \boldsymbol{\tau}^T, \quad \boldsymbol{P}\boldsymbol{F}^T = \boldsymbol{F}\boldsymbol{P}^T, \quad \boldsymbol{S} = \boldsymbol{S}^T} \tag{2.12}$$

for the Kirchhoff stress tensor, the First Piola-Kirchhoff stress tensor and the second Piola-Kirchhoff stress tensor, respectively.

2.2.4 Conservation of Energy: First Axiom of Thermodynamics

The energy balance is generally called the first law of thermodynamics, which is the main balance principle. In this principle, the progress of internal energy in a system is defined. Conservation of energy is expressed as,

$$\boxed{\frac{d}{dt}\int_{\mathcal{S}_t} \rho(e + \frac{1}{2}\boldsymbol{v}\cdot\boldsymbol{v})dv = \int_{\mathcal{S}_t} \rho(\boldsymbol{b}\cdot\boldsymbol{v} + r)dv + \int_{\mathcal{S}_t} (\boldsymbol{t}\cdot\boldsymbol{v} - h)da} \tag{2.13}$$

In the stated equation, e is the mass specific internal energy, r is the heat source generated by internal processes in the body and h is the outwards heat flux. The global form of of the internal energy balance takes the form

$$\frac{d}{dt}(\mathcal{K} + \mathcal{E}) = \mathcal{P} + \mathcal{Q}, \tag{2.14}$$

where $\mathcal{K}$, $\mathcal{E}$, $\mathcal{P}$ and $\mathcal{Q}$ are the kinetic energy, the internal energy, the mechanical power and non-mechanical power, respectively. The specific forms of the terms in equation (2.14) stated as,

$$\begin{aligned}
\mathcal{K} &:= \int_{\mathcal{S}_t} \frac{1}{2}\rho \boldsymbol{v}\cdot\boldsymbol{v} d\upsilon, \\
\mathcal{E} &:= \int_{\mathcal{S}_t} \rho e d\upsilon, \\
\mathcal{P} &:= \int_{\mathcal{S}_t} \rho \boldsymbol{b}\cdot\boldsymbol{v} d\upsilon + \int_{\partial\mathcal{S}_t} \boldsymbol{t}\cdot\boldsymbol{v} da, \\
\mathcal{Q} &:= \int_{\mathcal{S}_t} \rho r d\upsilon - \int_{\partial\mathcal{S}_t} h da.
\end{aligned} \tag{2.15}$$

Using all balance equations explained above, the local or strong form of the balance of internal energy is written as

$$\boxed{\rho\dot{e} + \operatorname{div}\boldsymbol{q} = \boldsymbol{\sigma} : \boldsymbol{d} + \rho r}, \tag{2.16}$$

where $\boldsymbol{d} := \operatorname{sym}[\boldsymbol{gl}]$ is the symmmetric part of the spatial velocity gradient $\boldsymbol{l} := \dot{\boldsymbol{F}}\boldsymbol{F}^{-1}$.

2.2.5 Clausius-Duhem Inequality: Second Axiom of Thermodynamics

The second law of thermodynamics restricts material equations governing elastic and inelastic dissipative mechanisms on the mechanical processes, and also restricts the direction of heat flow in thermal processes.

The entropy production is identified as the variation among the rate of entropy and the quantity heat received per unit temperature. Then, the Clausius-Duhem inequality is given as

$$\frac{d}{dt}\int_{\mathcal{S}_t} \rho\eta d\upsilon \geq \int_{\mathcal{S}_t} \frac{\rho r}{\theta} d\upsilon - \int_{\partial\mathcal{S}_t} \frac{h}{\theta} da \tag{2.17}$$

and it implies that rate of entropy increase must be greater than the entropy input rate. Through the Cauchy ($h = \boldsymbol{q}\cdot\boldsymbol{n}$) and the Gauss integral theorems we get

$$\boxed{\rho\dot{\eta} \geq \frac{\rho r}{\theta} - \operatorname{div}(\frac{\boldsymbol{q}}{\theta}) = \frac{\rho r}{\theta} - \frac{1}{\theta}\operatorname{div}\boldsymbol{q} + \frac{1}{\theta^2}\boldsymbol{q}\cdot\nabla_x\theta}. \tag{2.18}$$

2.3 Dissipation Inequality: Coleman's Method

The material equations are created such that they priori satisfy the second law of thermodynamics. After that, one can say that these equations are thermodynamically consistent. In other saying, the Clausius-Duhem Inequality (CDI) given in equation (2.18) enables as a restriction on the material equations. Using the local form of global balance of energy equation (2.16) in CDI equation, one can obtain,

$$\rho\gamma = \rho\dot{\eta} - \frac{1}{\theta}(\rho\dot{e} - \boldsymbol{\sigma} : \boldsymbol{d}) - \frac{1}{\theta^2}\boldsymbol{q} \cdot \nabla_x\theta \geq 0 \tag{2.19}$$

The dissipation at a material point, in other names, modified form of CDI is defined as

$$\mathcal{D} := \theta\gamma = \dot{\eta} - (\dot{e} - \frac{1}{\rho}\boldsymbol{\sigma} : \boldsymbol{d}) - \frac{1}{\rho\theta}\boldsymbol{q} \cdot \nabla_x\theta \geq 0 \tag{2.20}$$

The dissipation is decomposed into two stronger statements, local and conductive parts. Both of them are postulated to be greater than zero

$$\mathcal{D} = \mathcal{D}_{loc} + \mathcal{D}_{con} \geq 0, \tag{2.21}$$

where

$$\rho\mathcal{D}_{loc} := \boldsymbol{\sigma} : \boldsymbol{d} - \rho\dot{e} + \rho\theta\dot{\eta} \geq 0 \tag{2.22}$$

and

$$\rho\mathcal{D}_{con} := -\frac{1}{\theta}\boldsymbol{q} \cdot \nabla_x\theta \geq 0. \tag{2.23}$$

The stronger conditions given in equations (2.22) and (2.23) are referred to as the Clausius-Planck Inequality (CPI) and the Fourier Inequality (FI), respectively.
In solid mechanics, Helmholtz free energy is used as an alternative to the internal energy e. Using the Legendre transformation, the Helmholtz free energy is defined as

$$\Psi := e - \theta\eta. \tag{2.24}$$

The time derivative of the internal energy in CPI can be replaced with

$$\dot{e} = \dot{\Psi} + \eta\dot{\theta} + \theta\dot{\eta}. \tag{2.25}$$

Insertion of the latter into equation (2.22) results in

$$\rho\mathcal{D}_{loc} := \boldsymbol{\sigma} : \boldsymbol{d} - \rho\dot{\Psi} - \rho\eta\dot{\theta} \geq 0, \tag{2.26}$$

as the alternative form of the CPI. The equations (2.23) and (2.26) enforce the fundamental thermodynamic restriction on constitutive equations.

In general formulation of inelasticity problem, the Helmholtz free energy function and the heat flux is defined as

$$\Psi = \hat{\Psi}(\boldsymbol{X}, \boldsymbol{F}, \theta, \boldsymbol{\mathcal{I}}, \boldsymbol{g}) \quad \boldsymbol{q} = \hat{\boldsymbol{q}}(\boldsymbol{X}, \theta, \boldsymbol{F}, \boldsymbol{g}) \tag{2.27}$$

where $\boldsymbol{\mathcal{I}}$ is the generalized vector of internal variables and $\boldsymbol{g}$ is the temperature gradient. The time derivative of the Helmholtz free energy function becomes

$$\Psi = \partial_{\boldsymbol{F}}\Psi : \dot{\boldsymbol{F}} + \partial_{\theta}\Psi\dot{\theta} + \partial_{\boldsymbol{\mathcal{I}}}\Psi : \dot{\boldsymbol{\mathcal{I}}} + \partial_{\boldsymbol{g}}\Psi \cdot \dot{\boldsymbol{g}}. \tag{2.28}$$

Inserting this derivative in equation (2.26),

$$[J^{-1}\boldsymbol{P} - \rho\partial_{\boldsymbol{F}}\Psi] : \dot{\boldsymbol{F}} - \rho[\eta + \partial_{\theta}\Psi]\dot{\theta} - \rho[\partial_{\boldsymbol{\mathcal{I}}}\Psi] : \dot{\boldsymbol{\mathcal{I}}} - \rho[\partial_{\boldsymbol{g}}\Psi] \cdot \dot{\boldsymbol{g}} \geq 0 \tag{2.29}$$

is obtained. The expression, which is equivalent to stress power $\boldsymbol{\sigma} : \boldsymbol{d}$

$$\boldsymbol{\sigma} : \boldsymbol{d} = \boldsymbol{\sigma} : \boldsymbol{l} = J^{-1}\boldsymbol{P} : \dot{\boldsymbol{F}} = J^{-1}\boldsymbol{S} : \frac{1}{2}\dot{\boldsymbol{C}} = J^{-1}\boldsymbol{\tau} : \boldsymbol{d} \tag{2.30}$$

is used in equation (2.29).

The equality of equation (2.29) must be provided for arbitrary rates $\dot{\boldsymbol{F}}, \dot{\theta}$ and $\dot{\boldsymbol{g}}$. Thus, Coleman's method implies the particular form of material equations because we need

$$[\boldsymbol{P} - \rho_0\partial_{\boldsymbol{F}}\Psi] = \boldsymbol{0}, [\eta + \partial_{\theta}\Psi] = 0, [\partial_{\boldsymbol{g}}\Psi] = \boldsymbol{0}. \tag{2.31}$$

From these results, it is obviously seen that the Helmholtz free energy is not a function of temperature gradient. The free energy behaves as a potential for the stress and the entropy by way of

$$\boldsymbol{P} = \rho_0\partial_{\boldsymbol{F}}\Psi \quad \text{and} \quad \eta = -\partial_{\theta}\Psi \tag{2.32}$$

Therefore, the final form of local dissipation becomes

$$\rho\mathcal{D}_{loc} := -\rho[\partial_{\boldsymbol{\mathcal{I}}}\Psi] : \dot{\boldsymbol{\mathcal{I}}} = J^{-1}\boldsymbol{\beta} : \dot{\boldsymbol{\mathcal{I}}} \geq 0, \tag{2.33}$$

where $\boldsymbol{\beta} = -\rho_0\partial_{\boldsymbol{\mathcal{I}}}\Psi$ refers to thermodynamical force conjugate to the internal variables $\boldsymbol{\mathcal{I}}$ which represents flow owing to damage, viscosity and plasticity.

To sum up, for material modeling we only need to prescribe two constitutive functions, Helmholtz free energy Ψ and heat flux $\boldsymbol{q}$. The restrictions of these functions are equations (2.23) and (2.33).

CHAPTER 3

KINEMATICAL APPROACHES TO FINITE PLASTICITY OF SHAPE MEMORY POLYMERS

The kinematical approaches to the modeling of large viscoplastic deformation behaviour of glassy polymers are the topic of this chapter. Although there are many publications on metal plasticity kinematics, very few efforts have been made on the kinematic definition of amorphous glassy polymers. All the material models recommended for glass polymers take advantege from Kröner-Lee multiplicative decomposition of the deformation gradient $\boldsymbol{F} = \boldsymbol{F}^e \boldsymbol{F}^p$. Even though there have been previous studies on multiplicative split of the deformation gradient, in the work of Bilby et al. [13] the multiplicative decomposition of the deformation gradient in finite plasticity is the first time formally used. Bilby et al. [13] named total deformation gradient $\boldsymbol{F}$ as shape deformation, elastic deformation gradient $\boldsymbol{F}^e$ as lattice deformation and plastic deformation gradient $\boldsymbol{F}^p$ as dislocation deformation. After the seminal studies that Kröner and Lee made about this subject, multiplicative decomposition deformation gradient is commonly called as Kröner-Lee decomposition. This approach leads to stress free relaxed intermediate configuration. Miehe et al. [14] have proposed modular kinematic formulation in the logarithmic strain space for metal plasticity. In the later years, this work is extended to the finite viscoplasticity of glassy polymers by Miehe et al. [15] and [16]. First of all, the difficulties and assumptions from intermediate configuration are prevented from this framework, which also serves an effective algorithmic formulation and gives possibility to define basic kinematical setting for geometrically linear problem cases in the six dimensional symmetric space. In this chapter, these two references are used for kinematical approaches to glassy polymers.

3.1 Additive Kinematic Approach to Finite Plasticity in Logarithmic Strains

Various kinematical approaches such as the Kröner-Lee decomposition [46], [47], [48] and the Green-Naghdi theory [49] have been developed in the literature in order to formulate constitutive equations for elastic-plastic materials ongoing large strains. Kröner-Lee decomposition will be used due to the advantages stated at former section. To be coherent with Kröner-Lee decomposition, following form of a multiplicatively stated objective strain tensor enters the constitutive function for an elastic energy storage

$$\bar{\varepsilon}^e_y := \boldsymbol{f}_y(\boldsymbol{F}^{p-T}\boldsymbol{C}\boldsymbol{F}^{p-1}). \tag{3.1}$$

The convected current metric $\boldsymbol{C} := \boldsymbol{F}^T\boldsymbol{g}\boldsymbol{F} \in \text{sym}[3]_+$ is a function of deformation $\boldsymbol{F} \in GL[3]_+$ of the material and current metric $\boldsymbol{g}$, seen in Figure 3.1a. The Seth-Hill family of generalized strain measures are characterized by isotropic tensor function $\boldsymbol{f}_y$ as

$$\boldsymbol{f}_y(\boldsymbol{K}) = \begin{cases} \dfrac{1}{y}(\boldsymbol{K}^{y/2} - 1) & \text{if } y \neq 0 \\ \\ \dfrac{1}{2}\ln\boldsymbol{K} & \text{if } y = 0 \end{cases} \tag{3.2}$$

with $y \in \mathbb{R}$ and $\boldsymbol{K} \in \text{sym}[3]_+$. For isotropic and anisotropic materials with favoured structural directors which deform with material it can be shown that the plastic map enters the stored energy functions only through the metric $\boldsymbol{G}^p := \boldsymbol{F}^{pT}\tilde{\boldsymbol{G}}\boldsymbol{F}^p$. The Figure 3.1b introduces a framework of finite plasticity which depends on a plastic metric $\boldsymbol{G}^p$ entering the formulation as internal variable. In this framework, the intermediate configuration metric is defined as $\tilde{\boldsymbol{G}}$. The additive form of elastic Lagrangian strain tensor is identified as

$$\varepsilon^e_y := \boldsymbol{f}_y(\boldsymbol{C}) - \boldsymbol{f}_y(\boldsymbol{G}^p), \tag{3.3}$$

which depends on $\boldsymbol{C}$ and $\boldsymbol{G}^p$. According to the values of y calculated strain is changing. In the Lagrangian setting of finite elasticity, if $y = 0, 1, 2$ the equation gives the Hencky strain, the Biot strain and the Green strain, respectively. For the Green-Lagrangian strains with $y = 2$, when the invariants of the equation (3.3) are calculated

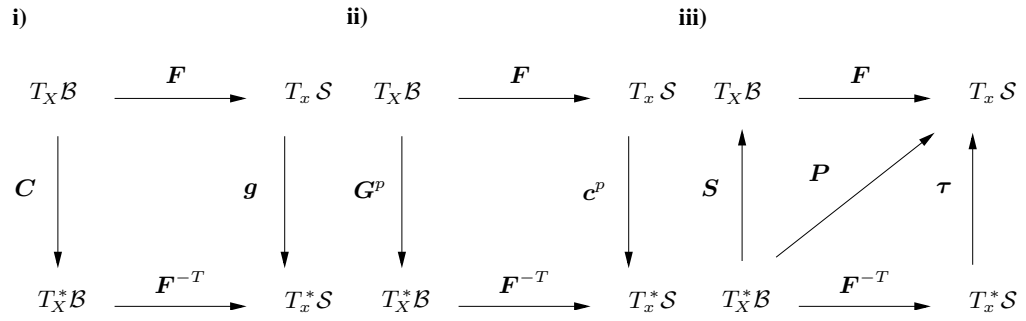

Figure 3.1: Mapping description of metric and stress tensors: i) Current metric $\boldsymbol{g}$ description in Lagrangian configuration, ii) plastic metric $\boldsymbol{G}^p$ description in Eulerian configuration, iii) nominal stress $\boldsymbol{P}$, Eulerian Kirchhoff stress $\boldsymbol{\tau}$, and the Lagrangian second Piola-Kirchhoff stress $\boldsymbol{S}$ definitions.

with reference to plastic metric, these invariants match up with invariants of the equation (3.1). On the other hand, using $y = 0$ in equations (3.1) and (3.3), it is observed that $\bar{\varepsilon}_0^e = \varepsilon_0^e$ for the special case of coaxial total and plastic deformations where $\boldsymbol{C}$ and $\boldsymbol{G}^p$ interchange and plastic map is defined as $\boldsymbol{F}^p = \boldsymbol{G}^{p1/2}$. In this regard, the logarithmic elastic strain measure in the Lagrangian setting is defined as

$$\boldsymbol{\varepsilon}^e := \frac{1}{2}\ln[\boldsymbol{C}] - \boldsymbol{\varepsilon}^p, \tag{3.4}$$

which makes additive form of equation (3.3) at least *"close"* to multiplicative form equation (3.1). In the constitutive formulations, the logarithmic plastic strain $\boldsymbol{\varepsilon}^p = (1/2)\ln\boldsymbol{G}^p$ may take in consideration as internal variable.

3.2 Modular Structure of the Constitutive Equations

The strain is additively decomposed to elastic and plastic parts in equation (3.4). This condition is the property of the geometrically linear theory of plasticity. Through the geometrically linear theory at finite strains, equation (3.4) also ensures that the constitutive structure has a material independent extension. According to Miehe et al. [14], the class of finite plasticity is defined by the following three modules; geometric pre-processor, constitutive model and geometric post-precessor.

- *Geometric pre-processor*: Using current and plastic metric, total and plastic logarithmic strain measures is defined, respectively.

- *Constitutive model*: Constitutive equations for (an)isotropic elasto-viscoplasticity in the logarithmic strain space is identified in a structure analogous to geometrically linear theory.
- *Geometric post-processor*: The objects obtained in logarithmic strain space are mapped back to their nominal, Eulerian or Lagrangian counterparts.

Adopting known costitutive models of the infinitesimal theory as a module in the logarithmic space makes that defined modular structure of finite plasticity interesting.

3.2.1 Current Metric, Plastic Metric and Nominal Stress

The right Cauchy Green tensor, which the Lagrangian representation of finite elasto-viscoplasticity bases on,

$$\boldsymbol{C} = \boldsymbol{F}\boldsymbol{g}\boldsymbol{F}^T \qquad \boldsymbol{C} \in \text{sym}[3]_+, \tag{3.5}$$

which is symmetric and positive definite. The pull-back operation of the Eulerian standard metric $\boldsymbol{g}$ to the Lagrangian setting defines this tensor as seen in Figure 3.1a. The definition of the inelastic deformation on covariant Lagrangian plastic metric $\boldsymbol{G}^p \in \text{sym}[3]_+$ can be seen in Figure 3.1b. Starting from beginning $t = t_0$, $\boldsymbol{G}^p$ is thought as an internal variable which is responsible for viscoplastic deformation

$$\boldsymbol{G}^p(t_0) = \boldsymbol{G}, \tag{3.6}$$

where $\boldsymbol{G}$ refers to the Lagrangian standard metric. The stress power

$$\mathscr{P}(t) := \boldsymbol{P} : \dot{\boldsymbol{F}} = \boldsymbol{S} : \frac{1}{2}\dot{\boldsymbol{C}} = \boldsymbol{\tau} : \frac{1}{2}\pounds_v \boldsymbol{g} \tag{3.7}$$

per unit reference volume of the material is identified as using non-symmetric nominal (first Piola) stress $\boldsymbol{P}$, the symmetric Lagrangian 2nd Piola stress $\boldsymbol{S}$ and Eulerian Kirchhoff stress $\boldsymbol{\tau}$. The time derivative of deformation gradient $\dot{\boldsymbol{F}}$, time derivative of Lagrangian right Cauchy Green tensor $\dot{\boldsymbol{C}}$ and the Lie derivative of Eulerian standard metric $\pounds_v \boldsymbol{g}$ are the work conjugate of defined stresses $\boldsymbol{P}$, $\boldsymbol{S}$ and $\boldsymbol{\tau}$, respectively.

3.2.2 Geometric Pre-processing of the Logarithmic Strain Space

To define an elastic strain measure ε^e is the critical part in the establishment of a framework of finite plasticity. The description of macroscopic energy storage is obtained under favour of this elastic stain measure.

$$\varepsilon^e = \varepsilon^e(\boldsymbol{C}, \boldsymbol{G}^p) \tag{3.8}$$

In the above definition, ε^e is the function of Lagrangian metric $\boldsymbol{C}$ and plastic metric $\boldsymbol{G}^p$. The additive form of elastic strain

$$\varepsilon^e := \varepsilon - \varepsilon^p \tag{3.9}$$

is also consistent with equation (3.4)

$$\boxed{\varepsilon := \frac{1}{2}\ln\boldsymbol{C} \quad \text{and} \quad \varepsilon^p = \frac{1}{2}\ln\boldsymbol{G}^p}, \tag{3.10}$$

where ε and ε^p are the logarithmic Lagrangian total and plastic strains, respectively. The multiplicative feature of large strain elastoplasticity is mapped by the logarithmic tensor function $\boldsymbol{f}_0$. The alteration of volume owing to plastic portion of the deformation is managed from the plastic Jacobian

$$J^p := \sqrt{\det[\boldsymbol{G}^p]} = \exp[\mathrm{tr}[\varepsilon^p]] \tag{3.11}$$

The plastic incompressibility is the most important part of the metal plasticity. This condition is also applicable for viscoplasticity in glassy thermoplastics. As a result, one can say that

$$\det[\boldsymbol{G}^p] = 1 \qquad \leftrightarrow \qquad \mathrm{tr}[\varepsilon^p] = 0. \tag{3.12}$$

As seen from above definitions, multiplicative constraint on the plastic metric $\boldsymbol{G}^p$ is defined as additive constraint on the logarithmic plastic strain ε^p. This property acts a critical role in selection of the logarithmic strain measures in equation (3.10). The logarithmic plastic strain measure ε^p can take into considiration as an internal factor alternative to $\boldsymbol{G}^p$ because there is one to one relationship between them. The definition of constitutive law is done in the logaritmic space. For this reason, there is no need to use geometric map in ε^p which is also considered as history variable in the constitutive law.

3.2.3 Definition of Transformation Tensors of the Logarithmic Space

The logarithmic strain measure $\boldsymbol{\varepsilon}$ shown in equation (3.10) is a function of $\boldsymbol{C}$ which depends on deformation gradient $\boldsymbol{F}$ and the Eulerian standard metric $\boldsymbol{g}$. The following relations are introduced to get sensitiveness of that strain measure regarding to alteration of deformation

$$\dot{\boldsymbol{\varepsilon}} = \mathbb{P} : \dot{\boldsymbol{F}} \quad \text{and} \quad \dot{\mathbb{P}} = \mathbb{L} : \dot{\boldsymbol{F}}, \tag{3.13}$$

where fourth and sixth order nominal transformation tensors are

$$\mathbb{P} := \partial_{\boldsymbol{F}} \boldsymbol{\varepsilon} \quad \text{and} \quad \mathbb{L} := \partial^2_{\boldsymbol{F}\boldsymbol{F}} \boldsymbol{\varepsilon} \tag{3.14}$$

respectively. In the treatment, these transformation tensors have very important place in the constitutive equations. Another description of the stress power can be obtained from putting the inverse of equation $(3.13)_1$ into equation $(3.7)_1$

$$\mathscr{P}(t) := \boldsymbol{\sigma} : \dot{\boldsymbol{\varepsilon}}, \tag{3.15}$$

where $\boldsymbol{\sigma} := \boldsymbol{P} : \mathbb{P}^{-1}$ is the Lagrangian stress tensor. This tensor is also work conjugate of the logarithmic strain measure $\boldsymbol{\varepsilon}$. The Lagrangian stress $\boldsymbol{\sigma}$ and logarithmic strain measure $\boldsymbol{\varepsilon}$ tensors are both symmetric. They are proper pair for external factors of the local material which is related with the logarithmic strain space.

3.2.4 Constitutive Model in the Logarithmic Strain Space

Hitherto, all the material model definitions are derived in the logarithmic strain space. Assuming a constitutive box, logarithmic strain measure $\boldsymbol{\varepsilon}$ and the set of internal variables such as $\boldsymbol{\varepsilon}^p$ in set $\boldsymbol{\mathcal{I}} := \{\boldsymbol{\varepsilon}^p, ...\}$ are given as an input. Using these input values, output of the constitutive box is obtained as current stress $\boldsymbol{\sigma}$ couple to the logarithmic strain and the corresponding elastoviscoplastic tangent moduli $\mathbb{E}^{algo}$

$$\boxed{\{\boldsymbol{\varepsilon}, \boldsymbol{\mathcal{I}}\} \quad \Rightarrow \quad MODEL \quad \Rightarrow \quad \{\boldsymbol{\sigma}, \mathbb{E}^{algo}\}} \tag{3.16}$$

Therefore, the structure of plasticity models of the geometrically linear theory can be protected from the constitutive model. Standard constitutive structure defined for small strain theory can be applied to the prepared model.

3.2.5 Geometric Post-processing of Nominal Stresses and Moduli

From the defined constitutive model in equation (3.16), the stresses and the corresponding tangent moduli in logarithmic spaces have been attained. These obtained variables are mapped to the nominal stresses and nominal moduli using predefined transformation tensors in Section 3.2.3. Considering $\boldsymbol{\sigma} := \boldsymbol{P} : \mathbb{P}^{-1}$ and equation (3.13)

$$\boxed{\boldsymbol{P} = \boldsymbol{\sigma} : \mathbb{P} \quad \text{and} \quad \mathbb{C}^{algo} = \mathbb{P}^T : \mathbb{E}^{algo} : \mathbb{P} + \boldsymbol{\sigma} : \mathbb{L}} \tag{3.17}$$

is obtained with regard to defined transformation tensors in equation (3.14). The sensitiveness of the nominal stresses with regard to the rate of deformation is directed from the fourth order nominal elastoviscoplastic tangent moduli $\mathbb{C}^{algo}$ as

$$\dot{\boldsymbol{P}} = \mathbb{C}^{algo} : \dot{\boldsymbol{F}}. \tag{3.18}$$

It is obvious that, the exponential map $\boldsymbol{G}^p = \exp[2\boldsymbol{\varepsilon}^p]$, also named as inverse of the logarithmic map equation $(3.10)_2$, is used to recover the plastic metric from logarithmic strain space. Thus, the significant stage of the constitutive structure of finite plasticity in the continuous setting is introduced in the boxed equations (3.10), (3.16) and (3.17).

3.2.6 Geometric Post-processing of Lagrangian and Eulerian Objects

The representation of the symmetric Lagrangian stresses $\boldsymbol{S} := \boldsymbol{F}^{-1}\boldsymbol{P}$ and its corresponding elastoviscoplastic moduli $\mathbb{C}_L^{algo}$ are showns as

$$\boldsymbol{S} = \boldsymbol{\sigma} : \mathbb{P}_L \quad \text{and} \quad \mathbb{C}_L^{algo} = \mathbb{P}_L^T : \mathbb{E}^{algo} : \mathbb{P}_L + \boldsymbol{\sigma} : \mathbb{L}_L. \tag{3.19}$$

They are derived from the nominal tensors introduced before. The definitions of the fourth order Lagrangian transformation tensor $\mathbb{P}_L$ and the sixth order Lagrangian transformation tensor $\mathbb{L}_L$ are

$$\mathbb{P}_L := 2\partial_{\boldsymbol{C}}\boldsymbol{\varepsilon} \quad \text{and} \quad \mathbb{L}_L := 4\partial^2_{\boldsymbol{CC}}\boldsymbol{\varepsilon}. \tag{3.20}$$

They are obtained as taking the derivative of logarithmic strain measure $\boldsymbol{\varepsilon}$ regarding to the current metric $\boldsymbol{C}$. The sensitiveness of the symmetric second Piola-Kirchhoff

stress according to the Lagrangian rate $\dot{\boldsymbol{C}}$ of deformation is governed from the fourth order Lagrangian consistent tangent moduli $\mathbb{C}_L^{algo}$ as

$$\dot{\boldsymbol{S}} = \mathbb{C}_L^{algo} : \frac{1}{2}\dot{\boldsymbol{C}}. \tag{3.21}$$

To be consistent with defined derivations $(3.17)_1$ and $(3.19)_1$, the Euler-Kirchhoff stress $\boldsymbol{\tau} = \boldsymbol{P}\boldsymbol{F}^T$ and its corresponding tangent moduli $\mathbb{C}_E^{algo}$ are defined as

$$\boldsymbol{\tau} = \boldsymbol{\sigma} : \mathbb{P}_E \quad \text{and} \quad \mathbb{C}_E^{algo} = \mathbb{P}_E^T : \mathbb{E}^{algo} : \mathbb{P}_E + \boldsymbol{\sigma} : \mathbb{L}_E. \tag{3.22}$$

The fourth order and sixth order Eulerian transformation tensors $\mathbb{P}_E$ and $\mathbb{L}_E$ are specified as

$$\mathbb{P}_E := 2\partial_{\boldsymbol{g}}\boldsymbol{\varepsilon} \quad \text{and} \quad \mathbb{L}_E := 4\partial^2_{\boldsymbol{g}\boldsymbol{g}}\boldsymbol{\varepsilon}, \tag{3.23}$$

respectively. They are the derivatives of the logarithmic strain measure according to the Eulerian standard metric $\boldsymbol{g}$. The Eulerian tangent governs the objective rate equation for the Lie dervative, which is defined as $\pounds_{\boldsymbol{v}}\boldsymbol{\tau} := \boldsymbol{F}\dot{\boldsymbol{S}}\boldsymbol{F}^T = \dot{\boldsymbol{\tau}} - \boldsymbol{l}\boldsymbol{\tau} - \boldsymbol{\tau}\boldsymbol{l}^T$, of the Kirchoff stress

$$\pounds_{\boldsymbol{v}}\boldsymbol{\tau} = \mathbb{C}_E^{algo} : \frac{1}{2}\pounds_{\boldsymbol{v}}\boldsymbol{g}. \tag{3.24}$$

$\pounds_{\boldsymbol{v}}\boldsymbol{g}$, frequently used as the Eulerian rate of deformation tensor, is the Lie derivative of the current metric $\boldsymbol{g}$. $\dot{\boldsymbol{F}}$ and $\boldsymbol{l} := \dot{\boldsymbol{F}}\boldsymbol{F}^{-1}$ are the material and spatial velocity grandients, respectively.

CHAPTER 4

CONSTITUTIVE MODEL FOR THERMOVISCOPLASTICITY

In this chapter, constitutive model characteristics of glassy polymers will be introduced. There are lots of situations which affect the characteristic behaviour of glassy polymers such as rate, pressure and the last but not the least temperature. The material also hardens at large deformations. Rheological representation of the material model can be seen in Figure 4.1.

The rheology of glassy polymers is modeled by two nonlinear springs and an Eyring-type dashpot. The first spring models the elastic recoverable stresses. The second spring is parallel to the Eyring-dashpot and it is responsible for post-yield hardening. In molecular setting, amorphous glassy polymers consist of long polymer chains. These chains are in a frozen-state due to secondary van der Waals type bonds. The elastic distortion of these bonds is modeled by the first spring in the Figure 4.1. As the material is stretched beyond a critical threshold, the viscoplastic dashpot is activated and the flow begins. As the material is stretched further, the long polymer chains are aligned in the direction of stretch. This induces a decrease in entropy and an increase in the free energy. Such a behaviour can be modeled in a similar way to rubber-like elasticity. For this reason, Arruda et al. [31] adopted the 8-chain model for the hardening branch, whereas Miehe et al. [16] uses the non-affine microsphere model.

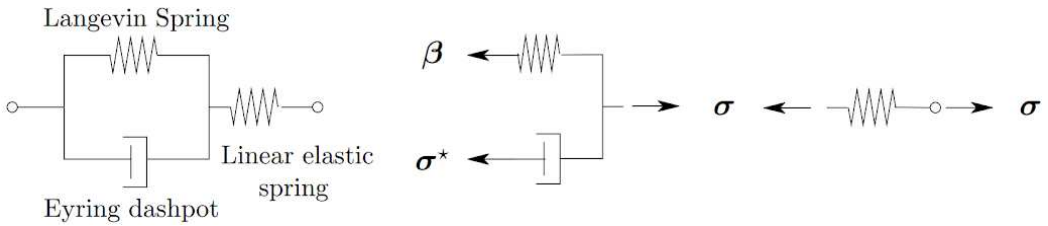

Figure 4.1: Rheological representation of the material model.

The molecular alignment of polymer chains causes post-yield hardening similar to the kinematic hardening observed in metal plasticity. As the material is heated, the secondary van der Waals bonds start to dissociate which causes softening in the elastic modulus and drop in the yield point. As the material is cold-drawn and heated, the yield point drops significantly near glass transition temperature. Hence, the aligned polymers start to retract to the energetically more favorable state causing the shape memory effect observed in thermoplastic materials.

First of all, general overview of material modeling in logarithmic strain space will be mentioned. The free energy function, total and back stress and the viscoplastic will be introduced throughtout this part. Secondly, splitted free energy function will be defined in detail. 8-chain model seen in Figure 4.2 is one of the network models that creates connection between small and large deformations by way of particular kinematical assumption. This model is derived from Arruda and Boyce [31] and it will be used in calculation for post yield kinematic hardening calculations. Using Arrhenius type equation and the double kink theory from Argon [21], the temperature dependent final form of flow rule will be obtained. Finally, thermal softening characteristic of the material will be desiganted. At the higher temperatures such as above the glass transition temperature T_g, glassy polymers soften and recover its undeformed shape. For this reason, softening mechanism is the most significant part of this chapter. Herein, the constitutive model and the evolution equations will be proposed in the logarithmic strain space as discussed in Chapter 3. Alternatively, one can use multiplicative kinematics in the sense of Kröner-Lee $\boldsymbol{F} = \boldsymbol{F}^e\boldsymbol{F}^p$ which can be utilized as well. However, such a treatment will require more elaborate operations for the update of the internal variables and tangent expressions, see for example Dal and Kaliske [45].

4.1 Constitutive Law in the Logarithmic Strain Space

The Helmholtz free energy function is formulated as a function of previously defined the total Hencky strain $\boldsymbol{\varepsilon}$ and the plastic strain $\boldsymbol{\varepsilon}^p$ in equation (3.10), and the absolute temperature θ in the additive form

$$\psi = \hat{\psi}(\boldsymbol{\varepsilon}, \boldsymbol{\varepsilon}^p, \theta) = \psi^e(\boldsymbol{\varepsilon} - \boldsymbol{\varepsilon}^p, \theta) + \psi^p(\boldsymbol{\varepsilon}^p, \theta) \tag{4.1}$$

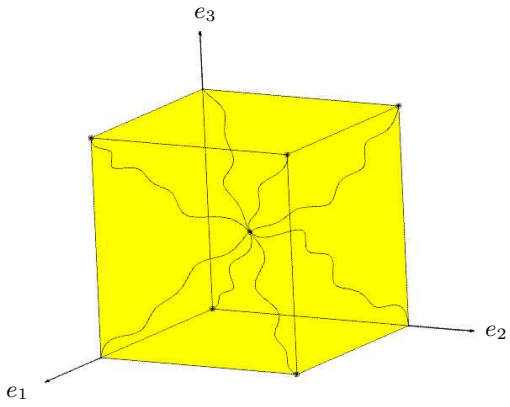

Figure 4.2: The 8-chain model of Arruda and Boyce [31]

per unit reference volume. The free energy equation is seperated into two parts. First, the elastic part ψ^e describes the stored energy owing to elastic deformations. Second, the plastic part ψ^p represents energy stored owing to plastic configuration change which behaves as a potential for back stresses. Using the Coleman's method expressed in Section 2.3 the total stress $\boldsymbol{\sigma}$ and the back stress $\boldsymbol{\beta}$ can be described as

$$\boldsymbol{\sigma} := \partial_{\boldsymbol{\varepsilon}} \psi^e(\boldsymbol{\varepsilon} - \boldsymbol{\varepsilon}^p) \quad \text{and} \quad \boldsymbol{\beta} := \partial_{\boldsymbol{\varepsilon}^p} \psi^p(\boldsymbol{\varepsilon}^p) \tag{4.2}$$

As a result of these definitions above, the local dissipation per unit reference volume has the form as

$$\mathcal{D}_{loc} := \boldsymbol{\sigma}^\star : \dot{\boldsymbol{\varepsilon}}^p \geq 0 \tag{4.3}$$

where $\boldsymbol{\sigma}^\star := \mathrm{dev}(\boldsymbol{\sigma} - \boldsymbol{\beta})$ with the definitions $\mathrm{dev}[(\bullet)] := (\bullet) - 1/3\,\mathrm{tr}[(\bullet)]\boldsymbol{1}$ and $\mathrm{tr}[(\bullet)] := (\bullet) : \boldsymbol{1}$. The evolution equation for the plastic strain $\boldsymbol{\varepsilon}^p$ need to be identified to complete the local overall constitutive framework. For this reason, the viscoplastic flow rule is introduced as

$$\dot{\boldsymbol{\varepsilon}}^p := \dot{\gamma}^p \frac{\boldsymbol{\sigma}^\star}{\|\boldsymbol{\sigma}^\star\|} \tag{4.4}$$

where $\|\bullet\| = \sqrt{(\bullet) : (\bullet)}$ stands for norm of a tensor and $\dot{\gamma}^p \geq 0$ must be satisfied in order to be thermodynamically consistent.

4.2 Specific Form of the Constitutive Equations

In the previous section, defined basic functions for the constitutive model are summarized as the elastic $\psi^e(\boldsymbol{\varepsilon} - \boldsymbol{\varepsilon}^p, \theta)$ and the plastic $\psi^p(\boldsymbol{\varepsilon}^p, \theta)$ part of the free energy

function and viscoplastic flow rule $\dot{\gamma}^p$. In this part, the introduction of these constitutive functions will be presented.

4.2.1 The Elastic Free Energy Function

Considering the whole deformations in polymers, elastic part is very small comparing with plastic part. Due to this reason, linear elasticity will be enough in the logarithmic strain space. Quadratic form of the free energy equation is defined as

$$\psi^e = \hat{\psi}^e(\boldsymbol{\varepsilon} - \boldsymbol{\varepsilon}^p, \theta) = \frac{\kappa}{2}\mathrm{tr}^2(\boldsymbol{\varepsilon} - \boldsymbol{\varepsilon}^p) + \mu\,\mathrm{dev}(\boldsymbol{\varepsilon} - \boldsymbol{\varepsilon}^p) : \mathrm{dev}(\boldsymbol{\varepsilon} - \boldsymbol{\varepsilon}^p) \tag{4.5}$$

in terms of the bulk modulus κ and shear modulus μ. Using previously defined equation (4.2), the stress expression in terms of strain is described as

$$\boldsymbol{\sigma} := -p\mathbf{1} + 2\mu\,\mathrm{dev}(\boldsymbol{\varepsilon} - \boldsymbol{\varepsilon}^p) \tag{4.6}$$

where $p := -\kappa\,\mathrm{tr}\,\boldsymbol{\varepsilon}^e$ represents the pressure term. According to Miehe and Lambrecht [17] and Bruhns et al. [18], the elastic strain $\boldsymbol{\varepsilon}^e$ is restricted due to ellipticity of the elastic free energy $\hat{\psi}^e$. For example, in the process of incompressible elasticity with a uniaxial test, maximum stretch λ value is restricted by $\lambda = \exp[1]$. Finite deformation in the analysis is applied below the glass transition temperature. Thus, $\lambda = \exp[1]$ is far below from the given deformations and this formulation does not have any contradiction with ellipticity neccessity.

4.2.2 The Plastic Free Energy Function

The viscoplastic kinematical hardening through the back stress is modeled from the plastic free energy function. Moreover, intramolecular resistance to the plastic flow feature of the material, which happens owing to chain allignment in the principal deformation direction, is obtained from the plastic free energy function. Haward and Thackray [19] states that the plastic free energy is taken from the theory of entropic rubber elasticity. This depends on toughness of the polymer chain. Then, the Langevin type plastic free energy function to model the post yield hardening is defined as

$$\psi^p = \hat{\psi}^p(\boldsymbol{\varepsilon}^p) = \mu_p N_p \left[\lambda_r^p \mathcal{L}^{-1}(\lambda_r^p) + \ln \frac{\mathcal{L}^{-1}(\lambda_r^p)}{\sinh \mathcal{L}^{-1}(\lambda_r^p)} \right] \tag{4.7}$$

where the shear modulus μ_p and the average segment number N_p are the material parameters in the constitutive relations. $\mathcal{L}^{-1}(*) := \coth(*) - 1/(*)$ is the Langevin function which is used in equation (4.7). λ_r^p is the macroscopic relative network stretch. The limited extensibility range of chains is kept down from this stretch. It has the form

$$\lambda_r^p = \sqrt{\frac{\lambda_1^{p2} + \lambda_2^{p2} + \lambda_3^{p2}}{3N_p}} \tag{4.8}$$

for 8-chain model. $\lambda_{i=1,2,3}^p$ are the principal isochoric plastic stretches. From the definition $\epsilon_a^p = \ln \lambda_a^p$, $\boldsymbol{\lambda}^p$ is described as

$$\boldsymbol{\lambda}^p := \exp(\boldsymbol{\varepsilon}^p) = \sum_{a=1}^{3} \lambda_a^p \, \boldsymbol{n}_a^p \otimes \boldsymbol{n}_a^p \tag{4.9}$$

where

$$\boldsymbol{\varepsilon}^p := \sum_{a=1}^{3} \epsilon_a^p \, \boldsymbol{n}_a^p \otimes \boldsymbol{n}_a^p \tag{4.10}$$

in terms of ϵ_a^p eigenvalue of plastic strain $\boldsymbol{\varepsilon}^p$ and $\boldsymbol{n}_a^p$ eigenvectorof the plastic strain $\boldsymbol{\varepsilon}^p$. For the derivation of back stress, Cohen [20] proposed the Padé approximation which is given as

$$\mathcal{L}^{-1}(\lambda_r^p) \approx \lambda_r^p \frac{3 - \lambda_r^p}{1 - \lambda_r^{p2}} \tag{4.11}$$

Using this approximation result, the back stress becomes,

$$\boldsymbol{\beta} = \sum_{a=1}^{3} \beta_a^p \, \boldsymbol{n}_a^p \otimes \boldsymbol{n}_a^p \quad \text{with} \quad \beta_a^p := \hat{\mu}_p(\lambda^p)\lambda_a^{p2} - \frac{1}{3}\sum_{a=1}^{3} \hat{\mu}_p(\lambda^p)\lambda_a^{p2} \tag{4.12}$$

where

$$\hat{\mu}_p(\lambda^p) := \frac{\mu_p}{3} \frac{3 - \lambda_r^{p2}}{1 - \lambda_r^{p2}} \tag{4.13}$$

4.2.3 Specification of the Flow Rule

The viscoplastic flow of glassy polymer is described by using the Arrhenius type equation

$$\dot{\gamma}^p = \dot{\gamma}_0 \exp(-\Delta G_f / k_B \theta) \tag{4.14}$$

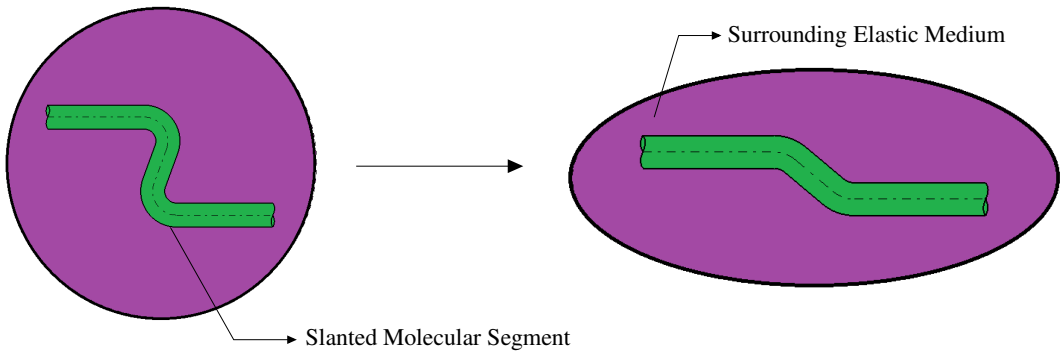

Figure 4.3: Unaligned and aligned molecular segments in double kink theory

in terms of Boltzman factor $\exp(-\Delta G_f/k_b\theta)$ where ΔG_f represents the energy barrier to start plastic flow or the activation free enthalpy. Double kink theory, depending on the wedge disclinations in Figure 4.3 and Figure 4.4, is defined in Argon [21] in order to evaluate ΔG_f. According to this theory, Argon creates a glassy polymer matrix which has zigzaggy molecular chain passed through one another producing an initially isotropic medium. These chains, first of all in an ordinary direction, are arranged to the direction of applied tensile load. At this stage, elastic medium is presumed to resist the plastic orientation. In order to get activation free enthalpy ΔG_f, reverse of loading explained above is applied. Elastic interaction of the molecules with its neighbours resists primarily the kink pair. The activation free enthalpy for formation of a pair of molecular kinks is obtained as subtracting the ΔW work done by externally applied shear stress $\boldsymbol{\tau}$ from ΔF the free energy of a wedge disclination loop. The kink pair model can be seen in Figure 4.5. ΔF, which depends on the distant stress field, was first obtained from Li and Gilman [22] as

$$\Delta F = 2\Delta F_{sing} - \Delta F_{inte} = \frac{3\pi a^3 \mu w^2}{16(1-\upsilon)} - \frac{9\pi w^2 a^3}{8(1-\upsilon)}\left(\frac{a}{z}\right)^5 \tag{4.15}$$

They have taken advantage of Volterra's Method [23] in order to determine the displacement field. In above equaiton ΔF_{sing} refers to free energy for a single disclination loop and ΔF_{inte} refers to interaction between two disclination loops having the same strength w and cylinder radius a. μ and υ are shear modulus and Poisson's ratio, respectively. As mentioned above, ΔW work done by the applied stress during the deformation is defined as

$$\Delta W = \pi a^3 w^2 \tau \left(\frac{z}{a}\right) \tag{4.16}$$

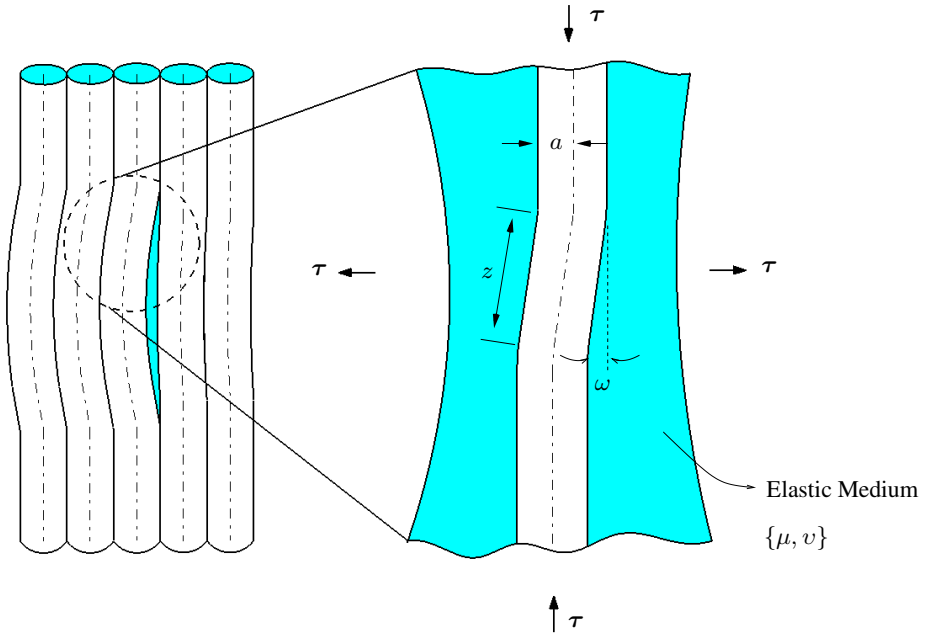

Figure 4.4: Pair of kinks form embedded in elastic matrix under an external stress field τ. (Reproduced from Miehe [16].)

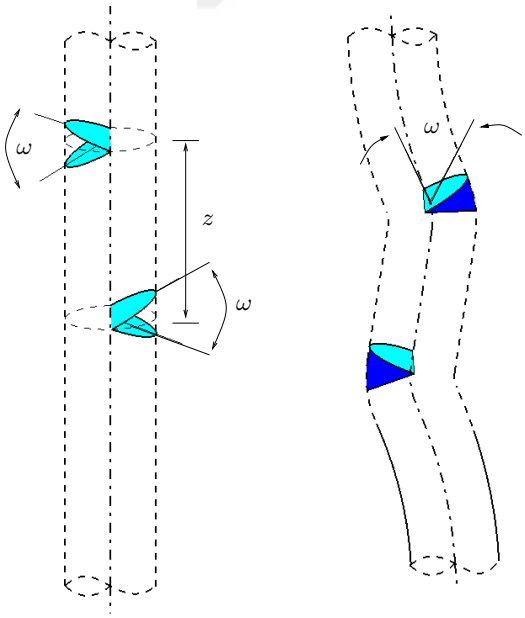

Figure 4.5: Pair of wedge disclination loops model for a molecular double-kink. (Reproduced from Miehe [16].)

Then, ΔG_f becomes

$$\Delta G_f = \Delta F - \Delta W = \frac{3\pi a^3 \mu w^2}{16(1-\upsilon)} - \frac{9\pi w^2 a^3}{8(1-\upsilon)}\Big(\frac{a}{z}\Big)^5 - \pi a^3 w^2 \tau\Big(\frac{z}{a}\Big). \quad (4.17)$$

Assuming constant applied stress, activation free enthalpy ΔG_f is a function of the seperation distance z and angle of rotation w between kinks. The ΔG_f expression is in quadratic form and has no extremum with respect to w. However, there is an extremum in z because the intermolecular interactions take over the intramolecular interactions assumption is done. Saddle point is obtained as taking derivative of free enthalpy expression, which τ/μ and w is constant, with respect to z/a and equating it to zero gives

$$\Big(\frac{z}{a}\Big)^\star = \left[\frac{45}{8(1-\upsilon)}\frac{\mu}{\tau}\right]^{1/6}. \quad (4.18)$$

Insert this expression in (4.17) and one obtains

$$\Delta G_f^\star = \frac{3\mu\pi a^3 w^2}{16(1-\upsilon)}\left[1 - \Big(\frac{\tau}{s_0}\Big)^{5/6}\right], \quad (4.19)$$

where $s_0 := 0.077\mu/(1-\upsilon)$ is the athermal shear strength and $\tau := \sqrt{J_2(\boldsymbol{\sigma}^\star)} = \sqrt{(\boldsymbol{\sigma}^\star : \boldsymbol{\sigma}^\star)/2}$ is the shear strength driving the viscoplastic element. Obtained $\Delta G_f^\star$ value is inserted into the Arrhenius equation, which yields the evolution law for the platic flow as

$$\dot{\gamma}^p := \dot{\gamma}_0 \exp\left[-\frac{As}{\theta}\left(1 - \Big\{\frac{\tau}{s_0}\Big\}^{5/6}\right)\right] \quad (4.20)$$

where $\dot{\gamma}_0$ and $A = 3\mu\pi a^3 w^2/16k_B(1-\upsilon)$ are the material parameters [21]. Boyce et al. [24] proposed a phenomenological evolution rule for s as

$$\boxed{\dot{s} := h(1 - s/s_{ss})\dot{\gamma}^p \quad \text{with} \quad s(0) = s_0} \quad (4.21)$$

where h refers slope of softening, s_0 and s_{ss} refers to initial and steady state values of athermal shear strength of s, respectively. The main purpose of this evalution rule is stated as to account for the strain softening and pressure dependency of yielding. Thus, the final form of the flow rule is obtained as

$$\boxed{\dot{\gamma}^p := \dot{\gamma}_0 \exp\left[-\frac{As}{\theta}\left(1 - \Big\{\frac{\tau}{s}\Big\}^{5/6}\right)\right]} \quad (4.22)$$

see also Argon [21].

4.3 Modeling of Mechanisms Describing the Thermal Softening

Mechanical properties of polymers depend on temperature. Increase in temperature results in thermal softening in the constitutive relations. In glassy polymers, intermolecular and intramolecular resistance are affected from temperature. Recalling the athermal shear strength which is defined as

$$s_0 := \frac{0.077\mu}{(1-\upsilon)}. \tag{4.23}$$

Decrease in shear strength of polymer under constant true strain rate is relevant with temperature dependence of elastic shear modulus μ. At this point, using the experimental results evolution for elastic shear modulus is proposed as

$$\boxed{\log(\mu) = \log(\mu_0) - \bar{c}(\theta - \theta_0)} \tag{4.24}$$

by Boyce et al. [25], which shows temperature dependent softening of the yield stress. The slope of $\log(\mu)$ vs Temperature gives $\bar{c}$.

The plastic shear modulus also depends on temperature. The following expression defined from Treloar [26]

$$\hat{\mu}_p(\theta) = \hat{n}_p(\theta) k_B \theta, \tag{4.25}$$

and it is derived from entropic polymer network theory. $\hat{n}_p(\theta)$, k_B and θ are the chain density, Boltzman constant and absolute temperature, respectively. The evolution of chain density of the plastic free energy is proposed as

$$\boxed{\hat{n}_p(\theta) = B - D\exp\left[\frac{-E_a}{R\theta}\right]}, \tag{4.26}$$

by Raha and Bowden [27] and Arruda [28]. R refers to the universal gas constant. B and D represent the material parameters and E_a defines the thermal dissociation energy. For the softening mechanism, it is not adequate to define only above relations. The mass equilibrium assumes that the molecular links number are constant

$$\boxed{\hat{n}_p(\theta)\hat{N}_p(\theta) = \hat{n}_p(\theta_0)\hat{N}_p(\theta_0) = constant}, \tag{4.27}$$

where $\hat{n}_p(\theta)$ is the chain density and $\hat{N}_p(\theta)$ is the number of segments per chain, respectively. For the derivation Boyce [29] can be checked. As seen from above derivations, the strain hardening of glassy polymers formed by entanglements parameters

n_p and N_p are thought as temperature dependent. Introduced equations (4.26) and (4.27) complete the temperature dependent hardening behaviour of glassy polymers. On the other hand, when reaching the glass transition temperature T_g, $\hat{n}_p(\theta_g) = 0$, therefore the relation between B and D is obtained as

$$\frac{B}{D} = \exp\left[\frac{-E_a}{RT_g}\right], \tag{4.28}$$

see also Basu et al. [30].

CHAPTER 5

ALGORITHMIC SETTING OF THE MODEL

Up to now, all the necessary derivations have been made for material model definitions. In this chapter, implementation of created material model to ABAQUS UMAT interface will be introduced. First of all, internal variables will be defined. Then, the algorithmic tangent moduli will be idendified. The ABAQUS term tangent moduli will be added to the previously described tangent moduli. Finally all the algorithm structure will be shown in Table 5.1.

Discrete time steps, $\Delta t = t_{n+1} - t_n$, will be used for evolution equation identification. The state variables at time t_n will be given as an input. Moreover, these will be indicated with subscript n.

5.1 Update of Internal Variables

There are two parameters to be updated in material model. One of them, athermal shear strength, is obtained from fully explicit numerical integration of equation (4.21). Then, athermal shear strength is defined as

$$s = s_n + \Delta t h(1 - s_n/s_{ss})\dot{\gamma}_n^p. \tag{5.1}$$

Another parameter to be updated is plastic strain tenson $\boldsymbol{\varepsilon}^p$ which is obtained by fully implicit update of equation (4.4). Euler updated for $\boldsymbol{\varepsilon}^p$ gives us

$$\boldsymbol{\varepsilon}^p = \boldsymbol{\varepsilon}_n^p + \Delta t \dot{\gamma}^p \boldsymbol{N} \qquad \text{with} \qquad \boldsymbol{N} := \frac{\boldsymbol{\sigma}^\star}{\|\boldsymbol{\sigma}^\star\|}. \tag{5.2}$$

The local Newton type isterative update shape is used in update equation of the plastic strain which is non-linear. The reason of non-linearity is the implicit dependencies of

Table 5.1: Flowchart of algorithmic update of the plastic strain

1. Get history/data base:
   i) History data: $\boldsymbol{\varepsilon}_n^p$, s_n, $\dot{\gamma}_n^p$, p_n
   ii) Current total strain : $\boldsymbol{\varepsilon}$

2. Explicit Update of the Athermal Shear Strength
   $s = s_n + \Delta t h(1 - s_n/s_{ss})\dot{\gamma}_n^p$

3. Implicit Update of the Plastic Strain
   i) Set number of iteration $i = 1$ and $tolerance = 10^{-10}$
   ii) Initialize
   $\boldsymbol{\varepsilon}^p|_{i=0} \leftarrow \boldsymbol{\varepsilon}_n^p$
   iii) Compute the dependent variables
   $\boldsymbol{\sigma}$, $\boldsymbol{\beta}$, $\boldsymbol{\sigma}^\star$, $\boldsymbol{N}$, τ, $\dot{\gamma}^p$
   iv) Compute the residual and its norm
   $\boldsymbol{r} = \boldsymbol{\varepsilon}^p - \boldsymbol{\varepsilon}_n^p - \Delta t \dot{\gamma}^p \boldsymbol{N}$ and $\|\boldsymbol{r}\| = \sqrt{\boldsymbol{r} : \boldsymbol{r}}$
   v) Compute the local tangent
   $\mathbb{a} := \partial_{\boldsymbol{\varepsilon}^p} \boldsymbol{r}$
   vi) Update the plastic strains
   $\boldsymbol{\varepsilon}^p \leftarrow \boldsymbol{\varepsilon}^p - \mathbb{a}^{-1} : \boldsymbol{r}$
   vii) Convergene check
   If $\|r\| \geq tolerance$
   $i \leftarrow i + 1$
   GO TO iii)
   ELSE
   Continue with 4

4. Store the history variables and proceed the Consistent Moduli

$\dot{\gamma}^p$ and $\boldsymbol{N}$ on the current valur of $\boldsymbol{\varepsilon}^p$. The detailed calculations for iterative method is shown in Appendix.

5.2 Algorithmic Tangent Moduli

Tangent moduli identification is very critical in material routines. It should be consistent with the internal variable update. The tangent moduli in the algorithm, sensitiveness of the stresses regarding to logarithmic strain, is defines as

$$\mathbb{E}^{Algo} = \mathrm{d}_{\boldsymbol{\varepsilon}} \boldsymbol{\sigma} = \mathbb{E}^e - 2\mu \partial_{\boldsymbol{\varepsilon}} \boldsymbol{\varepsilon}^p, \tag{5.3}$$

where $\mathbb{E}^e := \partial_{\boldsymbol{\varepsilon}}\boldsymbol{\sigma} = \kappa \boldsymbol{1} \otimes \boldsymbol{1} + 2\mu\mathbb{P}$ with $\mathbb{P} := \mathbb{I} - 1/3(\boldsymbol{1} \otimes \boldsymbol{1})$. The symmetric fourth-order identity tensor is defined as $\mathbb{I}$. Moreover, there is an additional part of the tangent moduli in ABAQUS. Detailed information about this part and sensitivity of the plastic strain tensor $\boldsymbol{\varepsilon}^p$ to the total strain tensor $\boldsymbol{\varepsilon}$ has been given in Appendix. After these definitions, algorithmic tangent moduli is derived as

$$\mathbb{E}^{Algo} = \mathbb{E}^e - 2\mu\Delta t\mathbb{a}^{-1} : \mathbb{h} : \mathbb{d}^e. \tag{5.4}$$

5.3 Algorithmic Implementation

All the algorithmic steps are summarized in this section. In the first step, history data and current total strain $\boldsymbol{\varepsilon}$ are given. Athermal shear strength is explicitly updated in the second step. In the third step, plastic strains are implicitly updated. The Newton-type iterative update is started with $i = 1$ and constrained with a tolerance value 10^{-10}. Plastic strains are set to their old values. Previously defined dependent variables are computed. Non-linear residual function and its norm are calculated from plastic strain equation. From calculated residual function, the local tangent is obtained. In the last part of step three, plastic strain in attained and convergence check is done. If the norm of the residual is higher than given tolerance, the algorith returns back to computation of the dependent variables. In order case, in a word the norm is less than given tolerance, the last step is continued. In the final step, step four, history variables are stored and consistent tangent moduli with ABAQUS term are proceeded.

CHAPTER 6

ILLUSTRATIVE NUMERICAL EXAMPLES

The main purpose of this chapter is to show the performance of the proposed material model which is implemented into ABAQUS as shown in Table 5.1. In the all examples, a poly (methyl methacrylate) (PMMA) will be used as a material. The properties of the material which is shown in Table 6.1 were taken from Dal [44]. While determining these material parameters, experimental data for PMMA in the literature at different temperatures was used. In order to get shape recovery, thermal softening part was added to the material model proposed by Dal [44].

In the first part of this chapter, verification of the proposed material model will be done with one element uniaxial compression test. Moreover, inhomogeneous tension and inhomogeneous compression tests for material model will be supplied to obtain results for complex loading cases. In the final part, temperature change effect in tube will be shown.

Table 6.1: Material parameters and universal constants required for the constitutive model

κ	=	2500	[MPa]	h	=	315	[MPa]
μ_0	=	1005	[MPa]	k_B	=	$1.38\text{x}10^{-20}$	[N-mm/K]
μ_{p_0}	=	15	[MPa]	$\bar{c}$	=	0.0016	[MPa/K]
N_{p_0}	=	2.7	[-]	B	=	$4.08\text{x}10^{18}$	[mm^{-3}]
$\dot{\gamma}_0$	=	$2.8\text{x}10^{7}$	[1/s]	D	=	$5.54\text{x}10^{21}$	[mm^{-3}]
A	=	100.6	[MPa/K]	R	=	1.9872	[Cal/mol-K]
α	=	$1.0\text{x}10^{-5}$	[K^{-1}]	E_a	=	5600	[Cal/mol]
θ_0	=	298	[K]	s_{ss}/s_0	=	0.83	[-]
ν	=	0.4392	[-]				

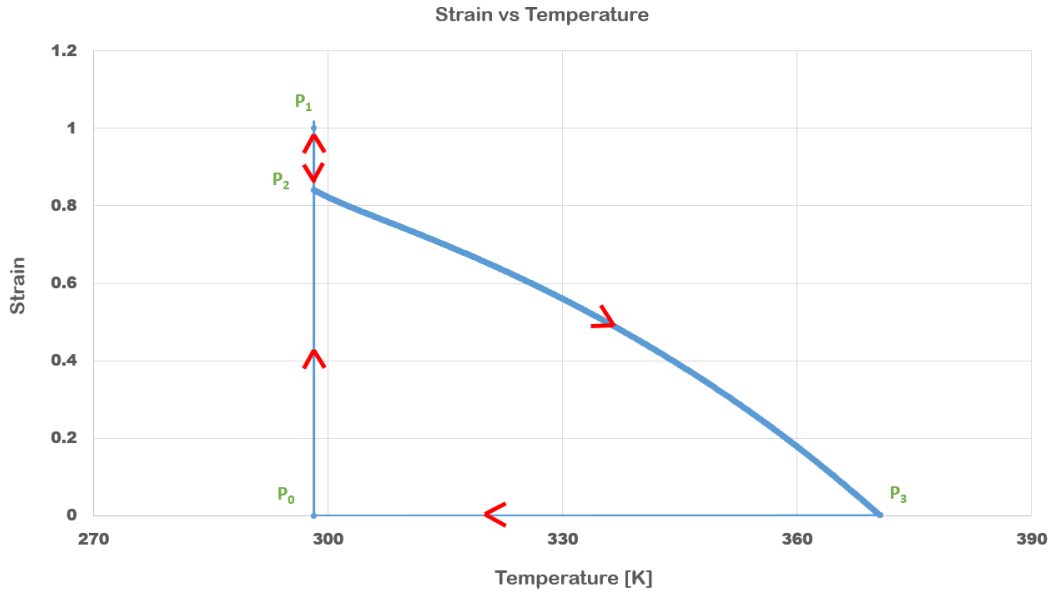

Figure 6.1: Strain-temperature curve for low temperature shape fixing and shape recovery

6.1 Validation of the Model

6.1.1 Uniaxial Compression Test

First of all, shape fixing and shape recovery capabilities of the material model were tested with one element cube model having $1mm$ length seen in Figure 6.2. In the first step P_0 to P_1, the displacement was applied as a boundary condition with the true strain rate of $\dot{\epsilon} = -0.001s^{-1}$ at $298K$. This process took 1000 seconds. In the second step P_1 to P_2, in order to recover elastic part of the strain, displacement boundary condition was unloaded keeping the temperature constant. In the third step P_2 to P_3, temperature was increased linearly $298K$ to $370K$ to get initial shape. In the final step P_3 to P_0, temperature was decreased to initial value. As previously defined in Chapter 1, this process is called as low temperature shape fixing and shape recovery. Strain change in these steps can be seen in Figure 6.1. Thus, shape recovery of the material model is working properly in this test.

In order to validate the proposed material model, experimental results of PMMA at different temperatures were taken from Arruda et al. [28]. They conducted uniaxial compression experiment on PMMA specimens. Their geometry was a cube which

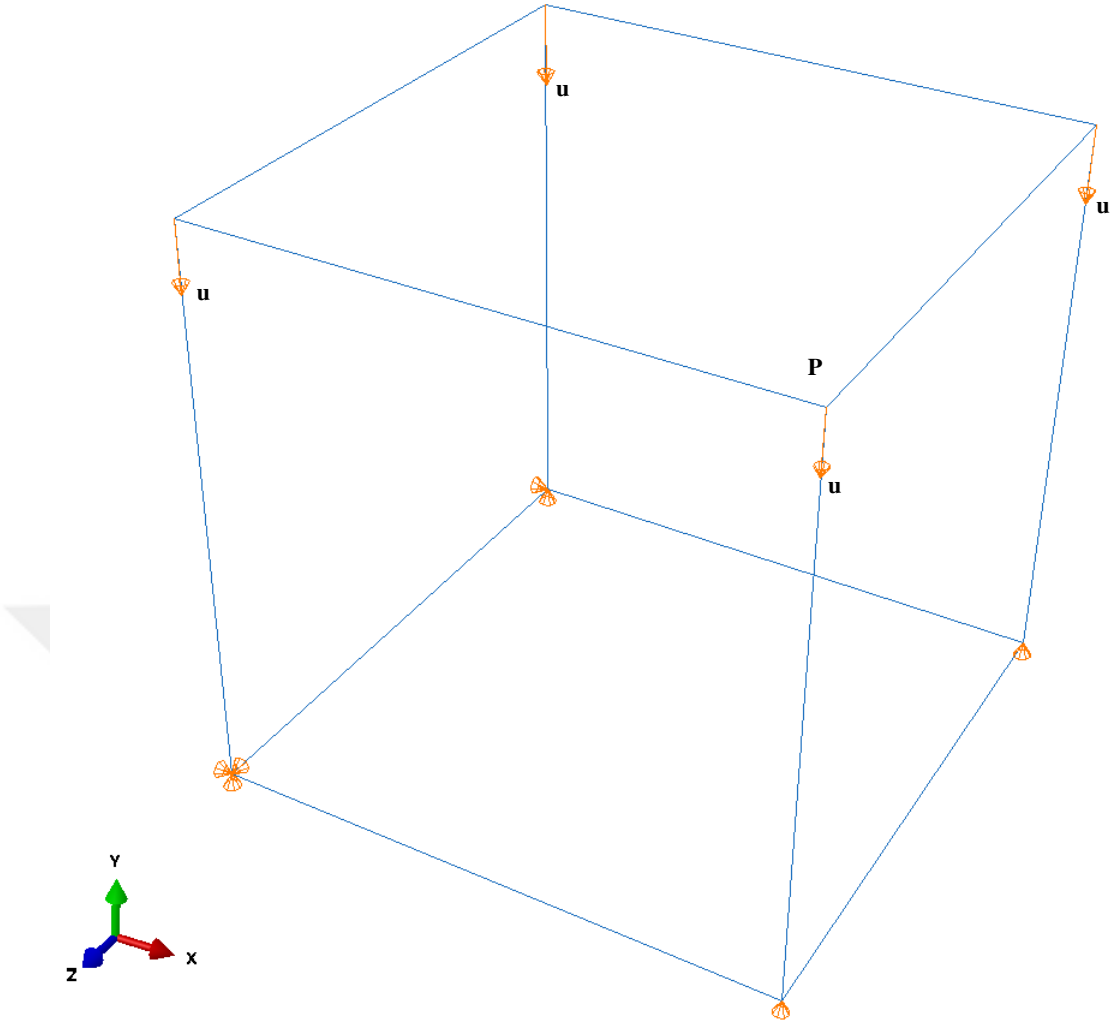

Figure 6.2: Finite element verification model. u and P denote the applied displacement direction and reference point, respectively

had $12.7mm$ length. They tested the specimen at the varying temperatures such as $298K$, $323K$ and $348K$ with the true strain rate of $\dot{\epsilon} = -0.001s^{-1}$.
Verification of UMAT is done with one element model which has a length of $1mm$. The element is uniaxially compressed with the strain rate of $\dot{\epsilon} = -0.001s^{-1}$. For this strain rate, simulation takes 1000 seconds in order to get $\epsilon = -1$. Separate models are created for different temperatures. The model can be seen in Figure 6.2. One point at the corner is chosen as reference that all the results are taken from. Reaction forces and displacements in y direction for the strains $\epsilon = -0.4$, $\epsilon = -0.6$ and $\epsilon = -1.0$ are shown in Figure 6.3. Time dependent reaction forces and displacements in x and z direction to calculate current area data are taken from reference point.

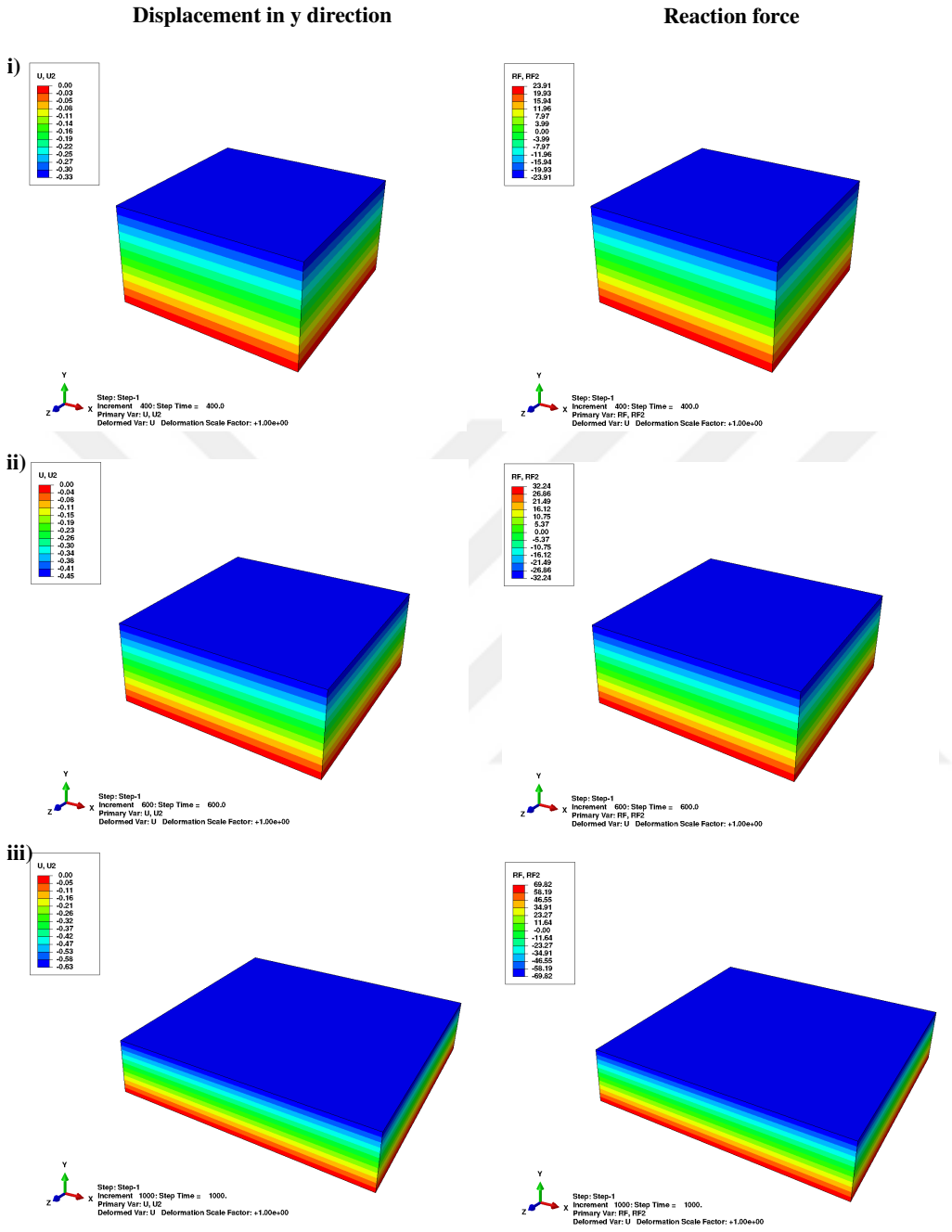

Figure 6.3: Reaction forces and displacements in y direction at 323 K: i) $\epsilon = -0.4$, ii) $\epsilon = -0.6$, iii) $\epsilon = -1.0$.

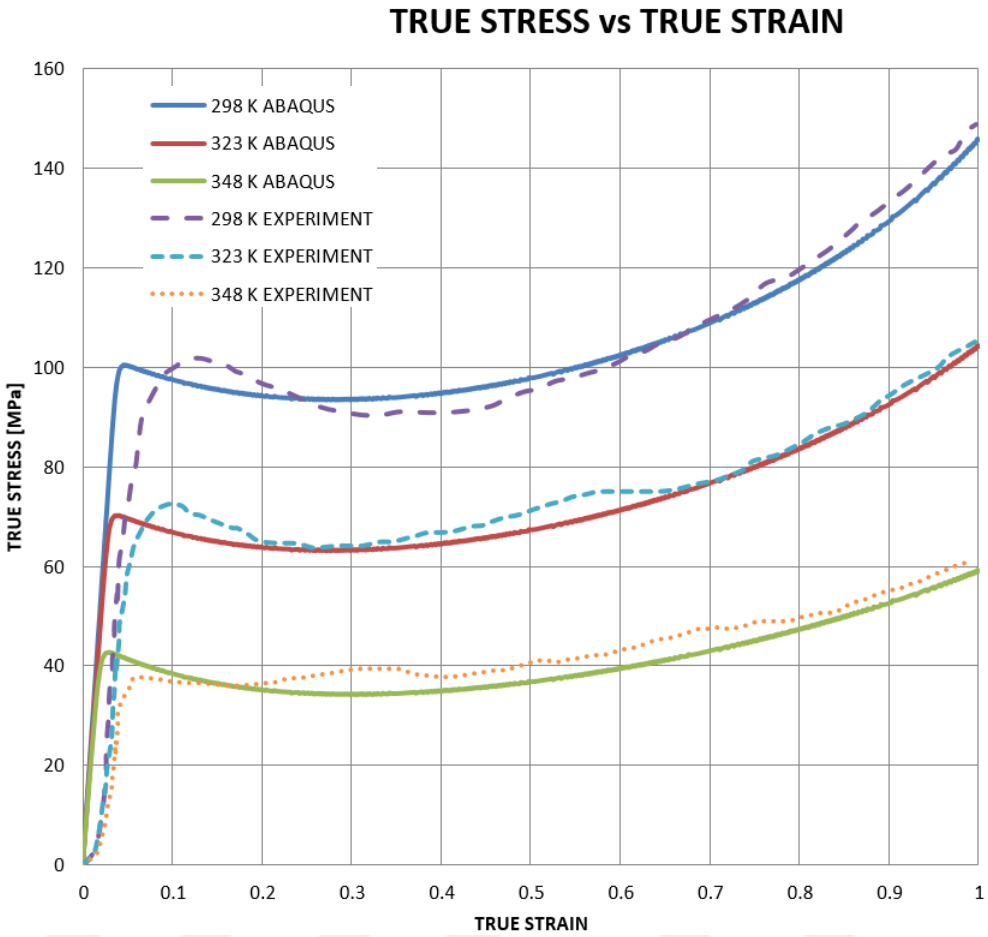

Figure 6.4: Comparison of the true stress-true strain curves for experiment [28] and the simulation results obtained from ABAQUS implementation.

The true stress is obtained from these data. Total force is four times the reaction forces because they are equal at the corners. As a result, true stress true strain data for experimental and analysis results at the material temperatures $293K$, $323K$ and $348K$ are plotted as shown in Figure 6.4. Because of the compressive loading, stresses and strains have negative value. However, the absolute values of the data are taken and plotted. It is obvious that peak values of the stresses at experiment and simulations match well. Increasing the temperature, the slope of the material curve is decreasing, which is great evidence to show working of softening mechanism. Thus, the proposed constitutive model can be used in more complicated problems.

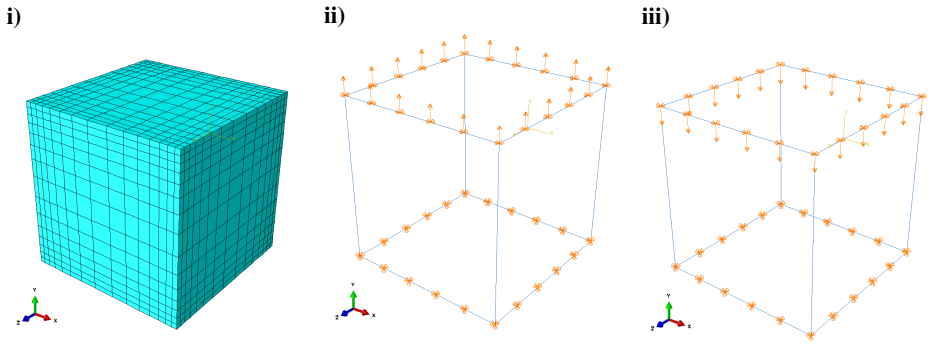

Figure 6.5: Model description for inhomogeneous tension and compresion: i) Mesh of the models, ii) inhomogeneous tension model, iii) inhomogeneous compression model.

6.1.2 Inhomogeneous Tension and Compression Test

After a successful uniaxial compression test comparison, inhomogeneous tension and inhomogeneous compression test models were also developed to support the written material model works properly. There is no experimental data to compare the results obtained from these models. In these analyzes, we wanted to show that the finite element models work under such loads as well.

First of all, a cube geometry with an edge of $50mm$ was created. With bias option, the geometry was meshed with more elements at the ends. The model has 3375 elements of the C3D20RH type. C3D20RH means that continuum three dimensional, 20-node quadratic brick, reduced integration, hybrid. Due to the incompressibility of the material and to reduce computation time hybrid and reduced integration option in the element has been chosen, respectively. Positive and negative $20mm$ displacements are applied as boundary conditions for tension and compression cases, respectively. For both cases, temperature was taken as $298K$ and model information can be obtained from the Figure 6.5. The stress and deformation results from the last step of loading can be seen in Figure 6.6. In order to demonstrate that the material model works under compressive load, the structure was allowed to deform excessively. For this reason, Von-Mises results in this case was limited to $500MPa$ to get rid of extreme stress plots at the corners. As a result, from the obtained great results for validation of written material model one can say that the material model can be used for more detailed analyzes.

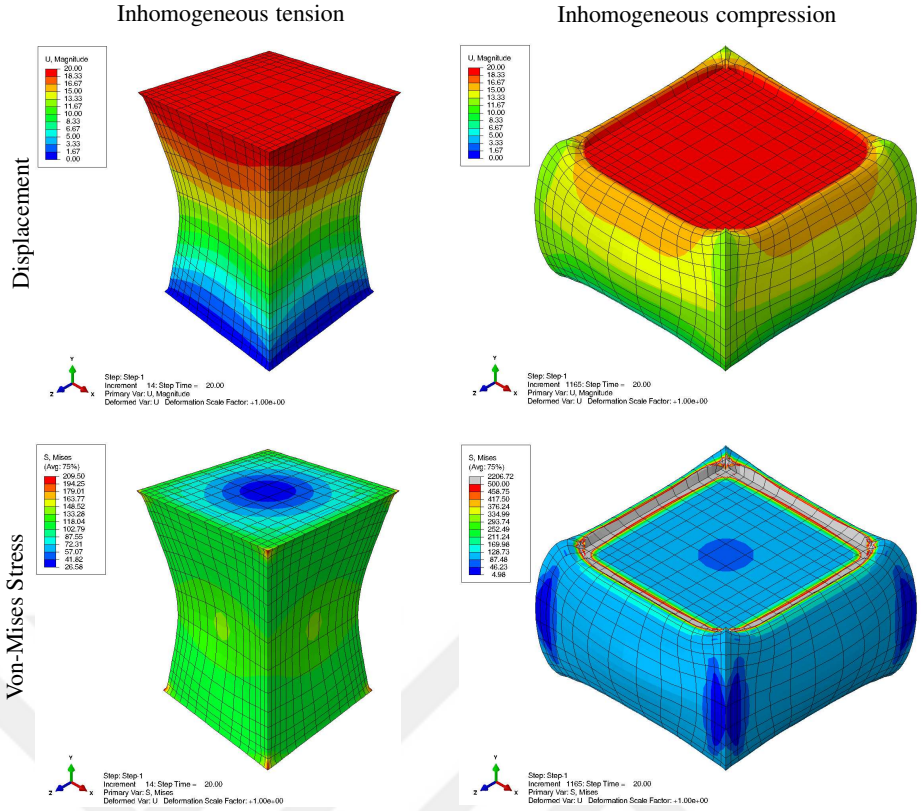

Figure 6.6: von-Mises stress and total displacement results.

6.2 Shape Recovery Example: Tube Model

Up to now, the generated material model was compared with the experimental results. As a result, the validity of the model was confirmed. After all the validation and verification, this section is devoted to show thermal softening and the shape memory mechanism of the generated material model.

In this section, a tube at room temperature given geometric dimensions in Figure 6.7 was compressed with the pressure load and deformed in the first step. In the second step, the tube was unloaded to compensate for the elastic deformation. In the last step, the tube was heated up to $380K$ slowly and waited for a long time so that it could take its first state. Maximum heated temperature was taken as $380K$ because above this temperature plastic shear modulus μ_p has negative value. This temperature is lower than glass transition temperature and there will be no phase change. However, elastic and plastic response of the material model causes shape recovery. The applied pressure and temperature change with respect to time can be seen in Figure 6.9. A number of modeling techniques were used to construct the finite element model. Due

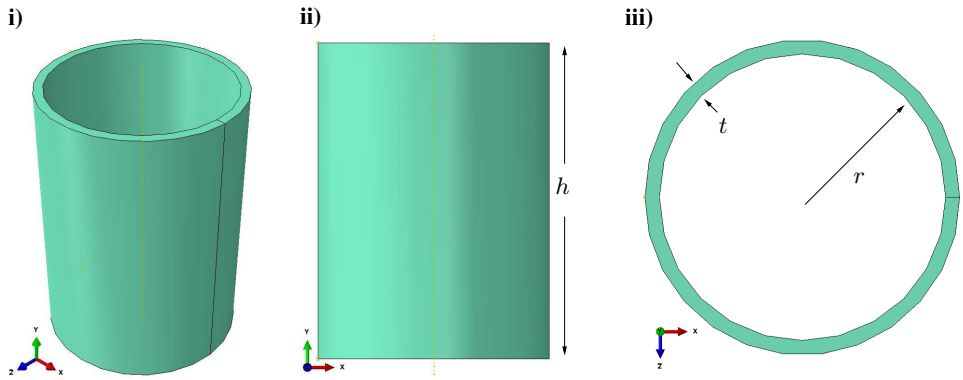

Figure 6.7: Geometry of the tube. Height, $h = 150mm$, tube thickness, $t = 5mm$, inner radius, $r = 50mm$: i) Isometric view, ii) side view, and iii) top view.

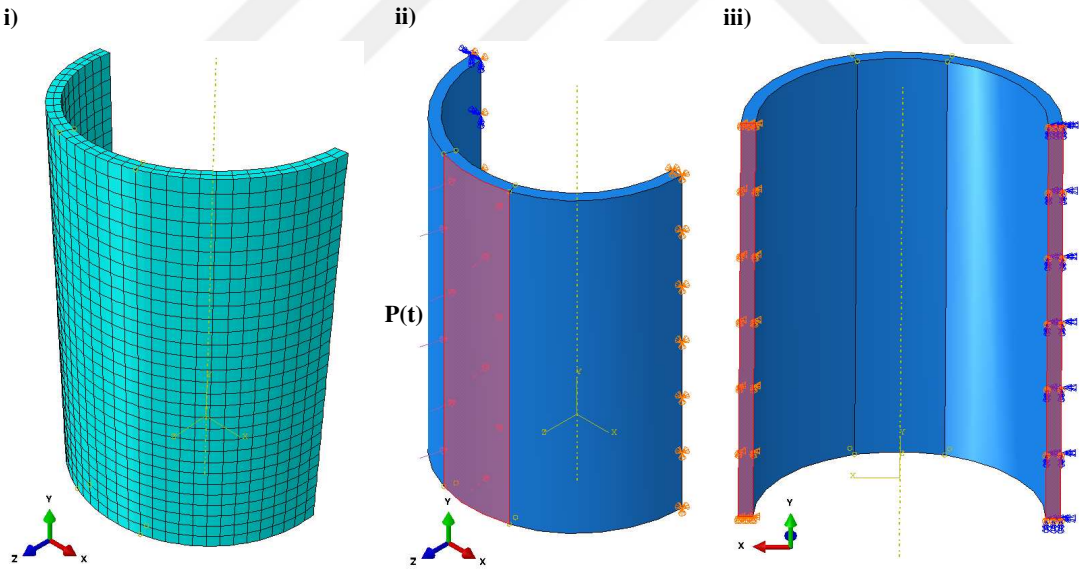

Figure 6.8: Finite element model of the tube: i) Mesh of the model, ii) pressure applied region, iii) applied boundary regions. Left surface is fixed at x,y and z. Right surface is fixed at z, rotation x (Rx) and rotation y (Ry).

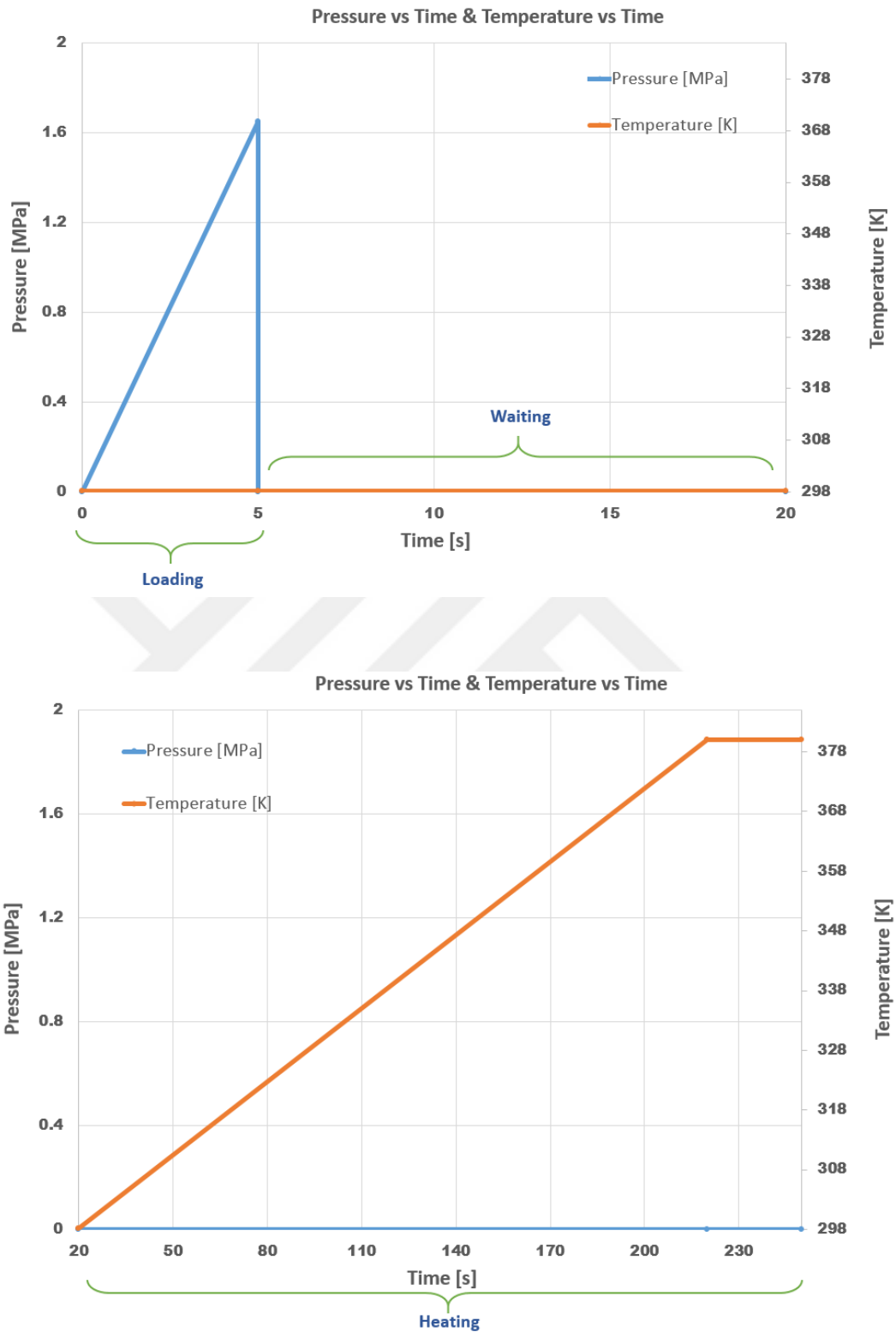

Figure 6.9: Pressure and temperature change with respect to time

to the symmetrical behavior of the part under load, only half of the part is modeled to decrease the resolution time and file sizes. The behavior of the other half was defined by boundary conditions. Mesh, applied pressure region and boundary condition of the model can be seen in the Figure 6.8. The model has 2100 elements of the C3D20RH type and in the thickness of the tube two rows of the elements were used.
All the stress and displacement in z direction results are shown in Figure 6.10. Despite the fact that half of the part was modelled, thanks to mirror result feature of ABAQUS, the result can be shown as a whole model. As the results show, most of the deformation is elastic, so the part is trying to get back to its original shape. However, when we look at the stress level, we can still see it is high after unloading. In the last step, after increasing the temperature and waiting for a long time, the part is still in shape recovery process and the stress level approaches almost zero. Therefore, the material behavior in this situation can be considered as non-ideal. As previously mentioned in Chapter 1, non-ideal materials are imperfect in shape recovery processes. Such shape memory polymers can be found in the literature extensively.

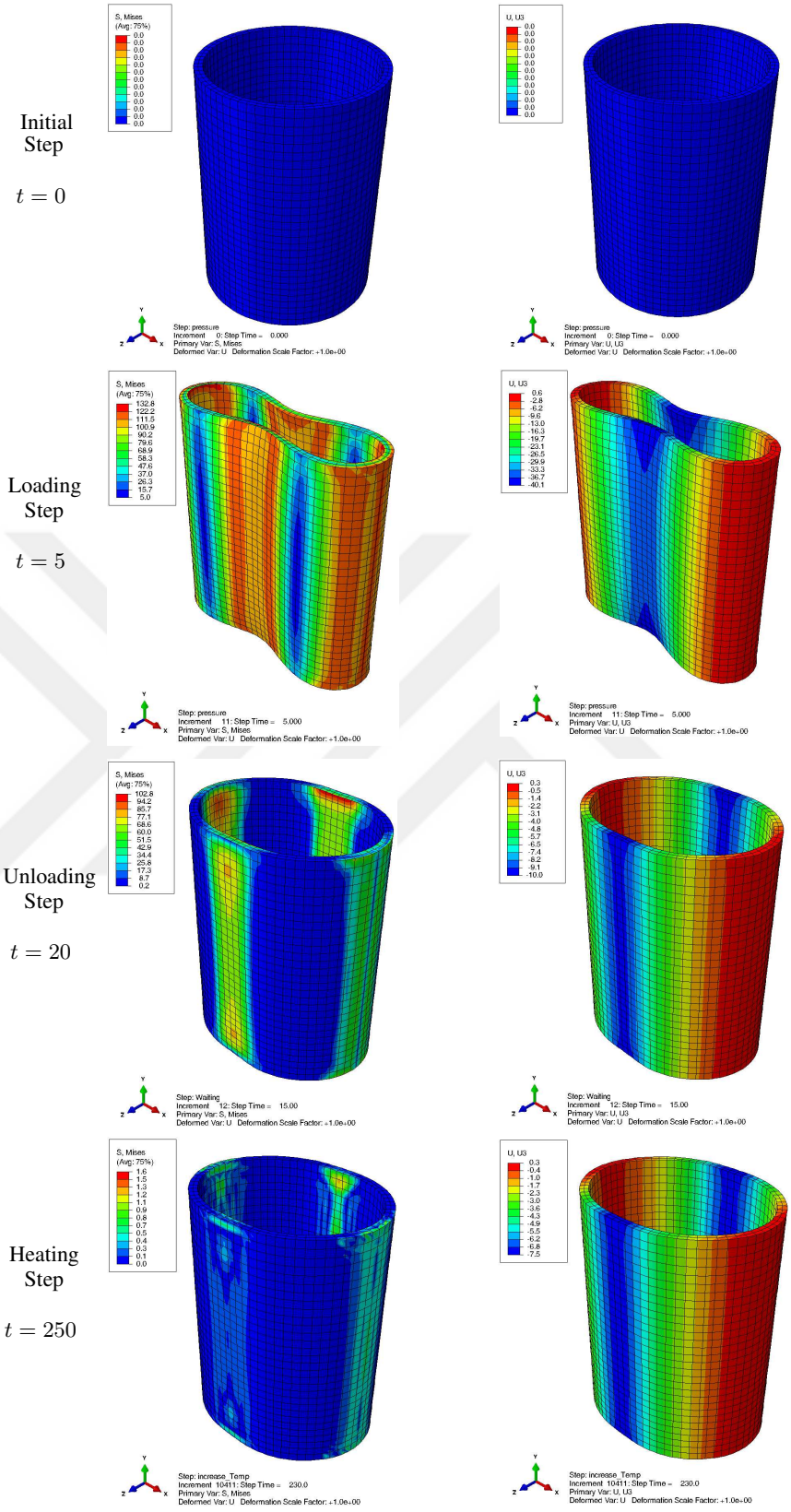

Figure 6.10: Distribution of von-Mises stress and displacement in z direction.

CHAPTER 7

CONCLUSION

In this thesis, a general information about shape memory characteristics of thermoplastic polymers has been given. The basics of continuum mechanics and kinematical approaches for the large deformation of glassy thermoplastics have been mentioned. The kinematic formulation previously defined for metal plasticity in the literature has been adapted for polymers. 8-chain model has been used to define flow rule and thermal softening mechanism of constitutive model. Algorithmic setting of the material model has been decribed. With the help of all these definitions, a user material that can be used in commercial analysis program ABAQUS has been generated. Finally, with the example given, the workability of the material model has been tested.

All these show us that using Argon's double kink theory, shape recovery can be modelled and glassy polymers have the shape memory ability. In the tube model, test runs were performed the temperatures between $298K$ and $380K$ in order to obtain temperature effect in material model. From these test runs, it was decided that the maximum temperature required for the shape recovery was $380K$ because above this temperature shear modulus μ_p has negative value. Although the maximum temperature capability of the material model is less than the glass transition temperature of the PMMA, elastic and plastic response of the material model causes shape recovery. Written material model is only working with solid elements in ABAQUS. As a more detailed finite element model, bumper of the car was modelled, however, due to quality reason such as aspect ratio, results could not be obtained. In this case, if the number of the element in the model is increased, "Illegal memory reference error" is taken. The number of cores used in ABAQUS runs can also cause this error. For example, you can get a solution with four cores while you do not have eight cores.

As a future work, based on this study, the generated material model can be developed

and adapted to more detailed models. This work will be useful in most areas because it has an ability to work with commercial software. In addition, the model can be developed further to work with shell elements.

REFERENCES

[1] L. B. Vernon, H. M. Vernon, 'Producing Molded Articles such as Dentures from Thermoplastic Synthetic Resins', *US Pat.*, 2234993

[2] W. C. Rainer, E. M. Redding, J. J. Hitov, A. W. Sloan and W. D. Stewart, 'Heat-shrinkable Polyethylene', *US Pat.*, 3144398, 1964.

[3] Chemical Economy & Engineering Reviews, Volume 16, 34 (1984).

[4] C. Liang, C. A. Rogers and E. Malafeew, "Investigation of Shape Memory Polymers and Their Hybrid Composites", Journal of Intelligent Material Systems and Structures, 8, 380 (1997).

[5] K. Nakayama, "Properties and Applications of Shape Memory Polymers", International Polymer Science and Technology, 18, 43 (1991).

[6] Y. Shirai and S. Hayashi, "Development of Polymeric Shape Memory Material", MTB184, Mitsubishi Heavy Industries, Inc., Japan, December (1988).

[7] M. Behl, A. Lendlein (2007,April). Shape-memory polymers. Materialstoday, 10, 20-28.

[8] Witold. M. Sokolowski, Artur B. Chmielewski, Shunichi Hayashi, and Toshido Yamada, "Cold hiberanated elastic memory (CHEM) self-deployable structures", SPIE Volume 3669, 179, (1999).

[9] D. K. Darooka, S. E. Scarborough, and D. P. Cadogan, "An Evaluation of an Inflatable Truss Frame for Space Applications", pages 3187-3197, American Institute of Aeronautics and Astronautics, AIAA-2001-1614 (2001).

[10] Dal, H. *Introduction to Continuum Mechanics*. Lecture Notes, Middle East Technical University, 2017.

[11] Göktepe, S. *Introduction to Computational Mechanics of Materials*. Lecture Notes, Middle East Technical University, 2015.

[12] Reddy, J. N. (2013). *An introduction to continuum merchanics.* Cambridge: Cambridge University Press.

[13] B. A. Bilby, L. R. T. Lardner, and A. N. Stroh. Continuous distributions of dislocations and the theory of plasticity. In *Actes du IXe congr'es international de m'ecanique appliqu'ee, (Bruxelles, 1956)*, volume 8, pages 35-44, 1957.

[14] Miehe, C. Apel, N. Lambrecht, M. (2002). *Anisotropic Additive Plasticity in the Logarithmic Strain Space: Modular Kinematic Formulation and Implementation Based on Incremental Minimization Principles for Standard Materials.* Computer Methods in Applied Mechanics and Engineering, 191: 5383-5425.

[15] Miehe, C. Göktepe, S. Mendez, J. (2005). *A Formulation of Finite ElastoViscoplasticity for Amorphous Glassy Polymers in the Logarithmic Strain Space.*.

[16] Miehe, C., Göktepe, S., Mendez, J. (2009). Finite viscoplasticity of amorphous glassy polymers in the logarithmic strain space. *International Journal of Solids and Structures, 46(1)*, 181-202. doi:10.1016/j.ijsolstr.2008.08.029

[17] Miehe, C., Lambrecht, M. (2001). Algorithms for computation of stresses and elastic moduli in terms of Seth-Hill's family of generalized strain tensors. Communications in Numerical Methods in Engineering 17, 337–353.

[18] Bruhns, O.T., Xiao, H., Meyers, A., 2001. Constitutive inequalities for an isotropic elastic strain energy function based on hencky's logarithmic strain tensor. Proceedings of the Royal Society London A 457, 2207–2226.

[19] Haward, R.N., Thackray, G., 1968. The use of a mathematical model to describe isothermal stress–strain curves in glassy thermoplastics. Proceedings of the Royal Society London A 302, 453–472.

[20] Cohen, A. (1991). A Padé approximant to the inverse Langevin function. Rheological Acta 30, 270–273.

[21] Argon, A. S. (1973). A Theory for the Low Temperature Plastic Deformation of Glassy Polymers. Philosophical Magazine, 28, 839-865.

[22] Li, J. C. M.; Gilman, J. J. (1970). Disclination Loops in Polymers. Journal of Applied Physics, 41, 4248-4256.

[23] Love, A. E. H. (1944). A Treatise on the Mathematical Theory of Elasticity. Dover Publications, New York.

[24] Boyce, M. C.; Parks, D. M.; Argon, A. S. (1988). Large Inelastic Deformation of Glassy Polymers. Part I: Rate Dependent Constitutive Model. Mechanics of Materials, 7, 15-33.

[25] Boyce, M. C.; Montagut, E. L.; Argon, A. S. (1992). The Effects of Thermomechanical Coupling on the Cold Drawing Process of Glassy Polymers. Polymer Engineering and Science, 32, 1073-1085.

[26] Treloar, L.R.G., 1975. The Physics of Rubber Elasticity, third ed. Clarendon Press, Oxford.

[27] Raha, S., Bowden, P.B., 1972. Birefringence of plastically deformed poly(methylmethacrylate). Polymer 13, 174–183.

[28] Arruda, E. M., Boyce, M. C., & Jayachandran, R. (1995). Effects of strain rate, temperature and thermomechanical coupling on the finite strain deformation of glassy polymers. *Mechanics of Materials,* 19(2-3), 193-212. doi:10.1016/0167-6636(94)00034-e

[29] Boyce, M. C. (1986). Large inelastic deformation of glassy polymers. Ph.D. thesis, The Massachusetts Institute of Technology.

[30] Basu, S., van der Giessen, E., 2002. A thermo-mechanical study of mode i, smallscale yielding crack-tip fields in glassy polymers. International Journal of Plasticity 18, 1395–1423.

[31] Arruda, E.M., Boyce, M.C., 1993. A three-dimensional constitutive model for the large stretch behavior of rubber elastic materials. Journal of the Mechanics and Physics of Solids 41, 389–412.

[32] Boatti, E., Scalet, G., Auricchio, F. (2016). A three-dimensional finite-strain phenomenological model for shape-memory polymers: Formulation, numerical simulations, and comparison with experimental data. *International Journal of Plasticity, 83,* 153-177. doi:10.1016/j.ijplas.2016.04.008

[33] Gall, K., Dunn, M. L., Liu, Y., Stefanic, G., Balzar, D. (2004). Internal stress storage in shape memory polymer nanocomposites. *Applied Physics Letters,* 85(2), 290-292. doi:10.1063/1.1769087

[34] Volk, B. L., Lagoudas, D. C., Maitland, D. J. (2011).Characterizing and modeling the free recovery and constrained recovery behavior of a polyurethane shape memory polymer. Smart Material Structure 20 (9), 094004-1-094004-18.

[35] Lendlein, A., Kelch, S., 2002. Shape-memory polymers. Angew. Chem. Int. Ed. 41, 2034-2057.

[36] Baghani, M., Arghavani, J., Naghdabadi, R. (2014). A finite deformation constitutive model for shape memory polymers based on Hencky strain. *Mechanics of Materials*, 73, 1-10. doi:10.1016/j.mechmat.2013.11.011

[37] Qi, H. J., Nguyen, T. D., Castro, F., Yakacki, C. M., and Shandas, R. (2008). Finite deformation thermo-mechanical behavior of thermally induced shape memory polymers. *Journal of the Mechanics and Physics of Solids*, 56, 1730-1751.

[38] Srivastava, V., Chester, S. A.,and Anand, L. (2010). Thermally actuated shape-memory polymers: Experiments, theory, and numerical simulations. *Journal of the Mechanics and Physics of Solids*, 58(8), 1100-1124. doi:10.1016/j.jmps.2010.04.004

[39] Diani, J., Gilormini, P., Frédy, C., and Rousseau, I. (2012). Predicting thermal shape memory of crosslinked polymer networks from linear viscoelasticity. *International Journal of Solids and Structures,* 49(5), 793-799. doi:10.1016/j.ijsolstr.2011.11.019

[40] Reese, S., Böl, M., and Christ, D. (2010). Finite element-based multi-phase modelling of shape memory polymer stents. *Computer Methods in Applied Mechanics and Engineering*, 199(21-22), 1276-1286. doi:10.1016/j.cma.2009.08.014

[41] Liu, C., Qin, H., and Mather, P. T. (2007). Review of progress in shape-memory polymers. *Journal of Materials Chemistry*, 17, 1543-1558. doi:10.1039/b615954k

[42] Dassault Systemes AD. *Abaqus User Guide*. 2014

[43] Bonet, J., & Wood, R. D. (2009). *Nonlinear continuum mechanics for finite element analysis.* Cambridge: Cambridge University Press.

[44] Dal, H. (2005). *Approaches to Modeling of Thermoviscoplastic Behavior of Glassy Polymers* (Unpublished master's thesis). Germany, University of Stuttgart.

[45] Dal, H., & Kaliske, M. (2009). Bergström-Boyce model for nonlinear finite rubber viscoelasticity: Theoretical aspects and algorithmic treatment for the FE method. *Computational Mechanics, 44(6),* 809-823. doi:10.1007/s00466-009-0407-2

[46] Kröner, E. (1959). Allgemeine Kontinuumstheorie der Versetzungen und Eigenspannungen. *Archive for Rational Mechanics and Analysis,* 4(1), 273-334. doi:10.1007/bf00281393

[47] Lee, E.H. (1969). Elastic-plastic deformation at finite strain. ASME Journal of Applied Mechanics 36, 1–6.

[48] Mandel, J. (1972). *Plasticite classique et viscoplasticite: Course held at the Department of mechanics of solids, September-October, 1971.* Wien: Springer.

[49] Green, A., Naghdi, P. (1965). A general theory of an elastic-plastic continuum. *Archive for Rational Mechanics and Analysis,* 18, 251–281.

APPENDIX A

USER MATERIAL ROUTINE (UMAT) IN ABAQUS

Material modeling is offered users to create their own material which are not available in ABAQUS library. In order to define the mechanical constitutive behavior of a material, user subroutine UMAT is used in ABAQUS. Any procedure which includes mechanical behaviour, UMAT can be used. It will be called at all material calculation points of elements for which the material definition includes a user-defined material behavior. It uses solution-dependent state variables which UMAT must update to their values at the end of the increment. In addition, UMAT must provide the material Jacobian matrix for the mechanical constitutive model [42]. Detailed information about UMAT can be obtained from Abaqus User Subroutines Reference Manual. Moreover, FORTRAN programming language have to be used in coding of ABAQUS user subroutines. One thing to note about FORTRAN is that the FORTRAN file extension varies according to the operating system used. In Linux or similar extension ".f" and in Windows or similar extension ".for" is used.

The most important part of the UMAT is to define properly stress and tangent moduli. ABAQUS uses different form of the total time derivative of the Kirchhoff stress. The Oldroyd rate of Kirchhoff stresses are equivalent to the Lie time derivative of Kirchhoff stresses.

$$\boldsymbol{\pounds}_v\boldsymbol{\tau} := \mathbb{C} : \frac{1}{2}\boldsymbol{\pounds}_v\boldsymbol{g} \quad \text{or} \quad \boldsymbol{\pounds}_v\boldsymbol{\tau} := \mathbb{C} : \boldsymbol{D} \quad \text{where} \quad \boldsymbol{D} := \frac{1}{2}(\boldsymbol{l} + \boldsymbol{l}^T) \tag{A.1}$$

By making use of $\mathbb{C} : \boldsymbol{D} := \mathbb{C} : \boldsymbol{l}$ the total time derivative of the Kirchhoff stresses becomes

$$\dot{\boldsymbol{\tau}} := \boldsymbol{\pounds}_v\boldsymbol{\tau} + \boldsymbol{l}\boldsymbol{\tau} + \boldsymbol{\tau}\boldsymbol{l}^T := \mathbb{C} : \boldsymbol{l} + \boldsymbol{l}\boldsymbol{\tau} + \boldsymbol{\tau}\boldsymbol{l}^T \tag{A.2}$$

The incremental form of the above expression is used as the tangent expression in ABAQUS as

$$\dot{\boldsymbol{\tau}} := \mathbb{E}_{Abaqus} : \boldsymbol{l} \quad \text{where} \quad \mathbb{E}^{abcd}_{Abaqus} := \mathbb{C}^{abcd} + \delta^{ac}\boldsymbol{\tau}^{bd} + \delta^{ad}\boldsymbol{\tau}^{bc} \tag{A.3}$$

where $\mathbb{C}^{abcd} = 2\partial_{\boldsymbol{g}}\boldsymbol{\tau}$ is the Eulerian tangent conjugate to the current metric $\boldsymbol{g}$. Therein, the term $\delta^{ac}\boldsymbol{\tau}^{bd} + \delta^{ad}\boldsymbol{\tau}^{bc}$ is added as an extra term to the material tangent expression. Recall $\boldsymbol{\tau} = J\boldsymbol{\sigma}$ the tangent term is modified as

$$\hat{\mathbb{E}}^{abcd}_{Abaqus} := \frac{1}{J}\mathbb{E}^{abcd}_{Abaqus} \tag{A.4}$$

The stress evolution

$$\Delta\boldsymbol{\sigma} := \hat{\mathbb{E}}^{abcd}_{Abaqus} : \Delta\boldsymbol{\varepsilon} \tag{A.5}$$

has to be symmetric. For this purpose, the tangent $\hat{\mathbb{E}}^{abcd}_{Abaqus}$ has to possess major and minor symmetries. Thus,

$$\begin{aligned} &\text{Major symmetry:} \quad \hat{\mathbb{E}}^{abcd}_{Abaqus} = \hat{\mathbb{E}}^{cdab}_{Abaqus} \\ &\text{Minor symmetry:} \quad \hat{\mathbb{E}}^{abcd}_{Abaqus} = \hat{\mathbb{E}}^{bacd}_{Abaqus} \quad \text{and} \quad \hat{\mathbb{E}}^{abcd}_{Abaqus} = \hat{\mathbb{E}}^{abdc}_{Abaqus} \end{aligned} \tag{A.6}$$

Applying the above mentioned symmetry constraints, tangent moduli is obtained as

$$\boxed{\hat{\mathbb{E}}_{Abaqus} = \frac{1}{J}(\mathbb{C} + \mathbb{E}_{sym}) \quad \text{where} \quad \mathbb{E}^{abcd}_{sym} = \frac{1}{2}(\delta^{ac}\tau^{bd} + \delta^{bd}\tau^{ac} + \delta^{ad}\tau^{bc} + \delta^{bc}\tau^{ad})} \tag{A.7}$$

The term $(1/J\ \mathbb{E}_{sym})$ is the additional term that is required in addition to the standard Eulerian tangent $\mathbb{C}$ for user material subroutine implementation UMAT into ABAQUS.

In the written subroutine followings are given as input

- deformation gradient for large deformations or strain tensor components for small deformations
- material parameters
- previous state (history) variables.

Outputs from these given inputs are

- stress tensor

- Jacobian matrix of constitutie model (Tangent Moduli)
- current state (history) variables.

As an example, the general format of the UMAT is shown in Figure A.1. The code is written for Neo-Hooke hyperelasticity. For the sake of brevity, only essential derivation parts are seen in in the figure. In fact, the code is longer and more complicated than it looks.

```
C-----------------------------------------------------------------------
C     UMAT FOR COMPRESSIBLE NEO-HOOKE HYPERELASTICITY
C-----------------------------------------------------------------------
      SUBROUTINE UMAT(STRESS,STATEV,DDSDDE,SSE,SPD,SCD,
     1 RPL,DDSDDT,DRPLDE,DRPLDT,
     2 STRAN,DSTRAN,TIME,DTIME,TEMP,DTEMP,PREDEF,DPRED,CMNAME,
     3 NDI,NSHR,NTENS,NSTATEV,PROPS,NPROPS,COORDS,DROT,PNEWDT,
     4 CELENT,DFGRD0,DFGRD1,NOEL,NPT,LAYER,KSPT,KSTEP,KINC)
C
      INCLUDE 'ABA_PARAM.INC'
C
      CHARACTER*8 CMNAME
      DIMENSION STRESS(NTENS),STATEV(NSTATEV),
     1 DDSDDE(NTENS,NTENS),DDSDDT(NTENS),DRPLDE(NTENS),
     2 STRAN(NTENS),DSTRAN(NTENS),TIME(2),PREDEF(1),DPRED(1),
     3 PROPS(NPROPS),COORDS(3),DROT(3,3),DFGRD0(3,3),DFGRD1(3,3)
C-----------------------------------------------------------------------
C     Material Properties
C-----------------------------------------------------------------------
      C10=PROPS(1)
      D1=PROPS(2)
C-----------------------------------------------------------------------
C     CALCULATE THE STRESS
C-----------------------------------------------------------------------
      DO K1=1,NDI
        STRESS(K1)=EG*(BBAR(K1)-TRBBAR)+PR
      END DO
      DO K1=NDI+1,NDI+NSHR
        STRESS(K1)=EG*BBAR(K1)
      END DO
C-----------------------------------------------------------------------
C     CALCULATE THE STIFFNESS
C-----------------------------------------------------------------------
      DO K1=1, NTENS
        DO K2=1, K1-1
          DDSDDE(K1, K2)=EG23*(BBAR(K1)+BBAR(K2)-TRBBAR)+EK
        END DO
      END DO
C
      DO K1=1, NTENS
        DO K2=1, K1-1
          DDSDDE(K1, K2)=DDSDDE(K2, K1)
        END DO
      END DO
C-----------------------------------------------------------------------
C     STORE ELASTIC STRAINS IN STATE VARIABLE ARRAY
C-----------------------------------------------------------------------
      DO K1 = 1, NTENS
        STATEV(K1) = EELAS(K1)
      END DO
C
C-----END OF UMAT
      RETURN
      END
C-----------------------------------------------------------------------
```

Figure A.1: Generated UMAT example for Neo-Hooke material model

APPENDIX B

ALGORITHMIC SETTING IF THE MATERIAL MODEL

B.1 Implicit Update of the Plastic Strain

In the algorithm, fully implicit update scheme is preferred for plastic strains $\boldsymbol{\varepsilon}^p$. Non-linear residual function $\boldsymbol{r}$ of the plastic strain tensor at the time step t_{n+1} is defined as

$$\boldsymbol{r}(\boldsymbol{\varepsilon}^p) := \boldsymbol{\varepsilon}^p - \boldsymbol{\varepsilon}^p_n - \Delta t \dot{\gamma}^p \boldsymbol{N} = \boldsymbol{0} \tag{B.1}$$

Iterative solution of the non-linear system requires linearization. Linearization of the residuum $\boldsymbol{r}$ at the i^{th} step is performed as

$$\operatorname{Lin} \boldsymbol{r}(\boldsymbol{\varepsilon}^p)|_{\boldsymbol{\varepsilon}^p_i} = \boldsymbol{r}(\boldsymbol{\varepsilon}^p_i) + \mathbb{a}_i : \Delta\boldsymbol{\varepsilon}^p = \boldsymbol{0} \tag{B.2}$$

where $\mathbb{a}_i := [\partial \boldsymbol{r}(\boldsymbol{\varepsilon}^p_i)]/[\partial \boldsymbol{\varepsilon}^p]$ is the local tangent. Solving the (B.2), update equation of $\boldsymbol{\varepsilon}^p$

$$\boldsymbol{\varepsilon}^p \quad \leftarrow \quad \boldsymbol{\varepsilon}^p_i - \mathbb{a}^{-1} : \boldsymbol{r}(\boldsymbol{\varepsilon}^p_i) \tag{B.3}$$

is obtained. Inserting (B.1) into the local tangent definition, the expression

$$\mathbb{a} = \mathbb{I} - \Delta t \mathbb{h} : \partial_{\boldsymbol{\varepsilon}^p} \boldsymbol{\sigma}^\star \tag{B.4}$$

is attained. The fourth order tensor

$$\mathbb{h} := \frac{\partial(\dot{\gamma}^p \boldsymbol{N})}{\partial \boldsymbol{\sigma}^\star} = (x_1 \mathbb{I} + x_2 \boldsymbol{N} \otimes \boldsymbol{N}) \tag{B.5}$$

is defined with the coefficients

$$x_1 := \frac{\dot{\gamma}^p}{\|\boldsymbol{\sigma}^\star\|} \quad \text{and} \quad x_2 := x_1 \left(\frac{5}{6} \frac{As}{\theta} \left\{ \frac{\tau}{s} \right\}^{5/6} - 1 \right) \tag{B.6}$$

The term

$$\partial_{\boldsymbol{\varepsilon}^p}\boldsymbol{\sigma}^\star = \partial_{\boldsymbol{\varepsilon}^p}\operatorname{dev}[\boldsymbol{\sigma}] - \partial_{\boldsymbol{\varepsilon}^p}\operatorname{dev}[\boldsymbol{\beta}] = -(\mathbb{d}^e + \mathbb{d}^p) \tag{B.7}$$

is described with

$$\mathbb{d}^e := \partial_{\boldsymbol{\varepsilon}}\operatorname{dev}[\boldsymbol{\sigma}]|_{\boldsymbol{\varepsilon}^p} = -\partial_{\boldsymbol{\varepsilon}^p}\operatorname{dev}[\boldsymbol{\sigma}]|_{\boldsymbol{\varepsilon}} = 2\mu\mathbb{P} \quad \text{and} \quad \mathbb{d}^p := \partial_{\boldsymbol{\varepsilon}^p}\operatorname{dev}[\boldsymbol{\beta}] \tag{B.8}$$

Thus, from the above definitions the local tangent is derived as

$$\mathbb{a} = \mathbb{I} + \Delta t\mathbb{h} : (\mathbb{d}^e + \mathbb{d}^p) \tag{B.9}$$

The detailed definitions of $\mathbb{d}^p$ for the eight-chain model the reader is referred to [16].

B.2 Sensitivity of the Plastic Strain

As referred earlier, sensitivity of plastic strain tensor to total strain tensor is used for tangent moduli identification. From equation (B.1), total derivative of the residuum function should be equal to zero at any moment of deformation. In other words,

$$\mathrm{d}_{\boldsymbol{\varepsilon}}\boldsymbol{r} = \partial_{\boldsymbol{\varepsilon}}\boldsymbol{r}|_{\boldsymbol{\varepsilon}^p} + \partial_{\boldsymbol{\varepsilon}^p}\boldsymbol{r}|_{\boldsymbol{\varepsilon}} : \partial_{\boldsymbol{\varepsilon}}\boldsymbol{\varepsilon}^p = \mathbb{0} \tag{B.10}$$

The definition of $\partial_{\boldsymbol{\varepsilon}^p}\boldsymbol{r}|_{\boldsymbol{\varepsilon}} = \mathbb{a}$ has been done before. The expression $\partial_{\boldsymbol{\varepsilon}}\boldsymbol{r}|_{\boldsymbol{\varepsilon}^p}$ has a form similar to (B.4) and can be identified as

$$\partial_{\boldsymbol{\varepsilon}}\boldsymbol{r}|_{\boldsymbol{\varepsilon}^p} = -\Delta t\mathbb{h} : \mathbb{d}^e \tag{B.11}$$

Therefore, from all the definitons above, the sensitivity of plastic strain to total strain can be expressed as

$$\partial_{\boldsymbol{\varepsilon}}\boldsymbol{\varepsilon}^p = -\Delta t\mathbb{a}^{-1} : \mathbb{h} : \mathbb{d}^e \tag{B.12}$$